# THE INFLUENCE OF SURFACE ROUGHNESS ON AIR-WATER INTERFACIAL AREAS IN POROUS MEDIA

**Ross Lieb-Lappen**
May 2007

Dr. Molly S. Costanza-Robinson
Thesis Advisor

Submitted in partial fulfillment of
**High Honors**
in
the Department of Chemistry and Biochemistry
and the Program of Environmental Studies
Middlebury College

Approved:

_____
Dr. Molly S. Costanza-Robinson (Advisor)

_____
Dr. Timothy Deschaines

_____
Dr. Peter Ryan

I hereby declare that I am the sole author of this thesis,
and that this thesis represents my own work in accordance with Middlebury College honor code.

***To my parents, for always believing in me.***

# ACKNOWLEDGEMENTS

First of all, I would like to thank Molly Costanza-Robinson for taking me into her lab and guiding me throughout this entire project. I had wide variety of interests and could not decide what I wanted to study. Molly has given me an amazing opportunity to try something new and has helped me tackle some of the obstacles along the way.

I would also like to thank the science support staff at Middlebury College, including Tony Desautels, Chris Goodrich, Gary Sprigg, and Tom Sheluga. I could not have completed this work without all of their continual help in the lab.

Thank you to all of my professors, especially my thesis committee, and fellow students at Middlebury. You have given me all of the tools and resources I have needed over the last four years, and will continue to use for the rest of my life. Thank you to my high school teachers as well for providing a solid foundation for my academics.

Most importantly, thank you to all of my family and friends. Your love and friendship are the most valuable possessions in my life. Thank you Lee for always being there to listen, provide insight, and help organize my schedule. Thank you to all of my grandparents for providing loving support throughout my life. Thank you mom, dad, and Mia because I know I can always count on you.

Finally, I would like to thank the Vermont Genetics Network and Middlebury College for funding this project.

# ABSTRACT

The air-water interface (AWI) is a critical parameter that influences the retention and transport of volatile contaminants through porous media, including soils. The areal extent of the AWI, $A_{ia}$, has been shown to vary with media texture and water saturation ($S_w$), with larger $A_{ia}$ values generally corresponding to increased adsorption capacity and retention of contaminants. The objective of this work is to characterize the $A_{ia}$–$S_w$ relationship using gas-phase interfacial tracer tests for two media: Vinton (fine sand with small amounts of silt and clay) and Granusil 7030 (fine sand). The media were chosen to represent two sands with similar particle sizes, but different surface roughness as represented by $N_2$/BET surface areas of 3.33 and 0.56 $m^2/g$, respectively. Media with greater surface roughness are hypothesized to yield larger interfacial areas, leading to increased retardation of contaminant transport. $A_{ia}$ was measured using decane vapor as the interfacial tracer for porous media at water saturations ranging from approximately 2.5% to 20%. Once $A_{ia}$ was measured for a particular system, its value was used to predict the gas-phase retardation of a contaminant, trichloroethylene (TCE) vapor, an industrial organic solvent and carcinogen, traveling through the same soil system. The predicted retardation for TCE was then compared to its observed retardation through the soil column. Results show that overall, $A_{ia}$ generally decreased with increasing $S_w$, in agreement with the literature. For all $S_w$ studied, measured $A_{ia}$ values were greater for Vinton than for Granusil 7030 as a result of the greater surface roughness for Vinton. Predicted retardation factors for TCE matched the general $S_w$ trend of the observed data, however, predictions were consistently greater than observed values. This difference is attributed to uncertainty in the interfacial adsorption coefficient for decane.

# TABLE OF CONTENTS

# TABLES



# FIGURES

**Chapter I**



**Chapter II**



**Chapter III**

## FIGURES – CONTINUED

**Chapter IV**

# I. INTRODUCTION AND BACKGROUND

*Importance of Understanding the Transport of Contaminants*

The growing production and consumption of chemicals during the last century has led to an increase in the quantity of volatile organic compounds (VOCs) in the vadose zone.[1] A 2006 aquifer study by the United States Geological Survey found VOCs at an assessment level of 0.2 μg/L in 19% of groundwater wells tested across the country. Although only 1-2% of the domestic and public wells had VOC concentrations above the maximum contaminant level (MCL), the long term health effects of low-level exposure to some VOCs are uncertain.[1] Common sources of these contaminants include accidental spills, poor waste management practices, and leaking underground storage tanks, all of which can pose serious human health risks, especially with regard to drinking water.[1]

VOCs are transported through the vadose zone as non-aqueous phase liquids (NAPLs), as dissolved solutes, or as vapor plumes. Although VOCs tend to have low aqueous solubility, aqueous concentrations can still easily exceed EPA regulations. The VOCs can then serve as long term sources of groundwater contamination.[1-2] Because of VOC volatility, VOC vapor plumes readily disperse, potentially affecting a much larger volume in the vadose zone.[1] The most common technique to remediate VOCs from the vadose zone, soil vapor extraction (SVE), exploits this volatility by purging the contaminated soil with air. This method is relatively cheap, simple, and can be applied at a wide range of spatial scales.[2-3]

Effective SVE remediation requires an understanding of gas-phase retention and transport of contaminants, such as VOCs, in porous media. This knowledge improves predictive capabilities, risk assessment, and subsequent remediation efforts.

*The Air-Water Interface*

The transport of any solute flowing through a soil system is retarded to some degree by five processes: sorption to the solid mineral phase, sorption to the soil organic matter (SOM), dissolution into bulk water, partitioning into NAPL, and accumulation at the air(gas)–water interface (AWI).[4-8] Previous studies indicate that if SOM is present, it is responsible for the majority of the solute retention. However, in systems with low SOM, solute retardation, R, is governed by multiple retention processes:

$$R = 1 + R_s + R_w + R_{ia} \qquad [1\text{-}1]$$

where $R_s$, $R_w$, and $R_{ia}$ represent the retardation due to adsorption to the solid-phase (mineral grains and SOM), dissolution into the aqueous phase, and adsorption at the AWI, respectively. At extremely low water saturations, adsorption to dry mineral surfaces dominates the retention of the solute.[4-8] In media with low concentrations of SOM and intermediate water saturations, the interplay among the retention domains is more complicated. Only recently has $R_{ia}$ been shown to be a critical parameter in select porous media systems. For example, in 1997, Brusseau et al.[5] attributed 29-73% of retardation of the contaminant trichloroethylene (TCE) to retention at the AWI. Furthermore, Hoff et al.[9] estimated that the AWI was responsible for up to 50% of the retention of straight-chain alkanes in a sandy aquifer material.

Previous research has demonstrated that the area of the AWI (air-water interfacial area, or $A_{ia}$) affects the kinetics and equilibrium retention of VOCs, bacteria and viruses, and inorganic colloids in a variety of environmental systems.[10-16] Depending on the soil texture and water content, $A_{ia}$ can vary among porous media, with larger values generally corresponding to increased adsorption capacity and retention for contaminants, and

possibly decreased mass-transfer rate limitations.[12] Wan and Wilson[13-14] identified the AWI as the preferential adsorption domain for colloids and developed a method for quantifying the adsorption coefficients. Using a similar method, Schäfer et al.[15] measured the accumulation of bacteria at the AWI, while Donaldson and Anderson[16] examined the adsorption of atmospheric gases to the AWI in fog.

*Adsorption at the Air-Water Interface*

Vapor adsorption at the AWI is exothermic and is considered a spontaneous process relative to other transport processes.[4,6] Thus, as a contaminant travels through a soil system, it is considered to be under equilibrium conditions with respect to interfacial adsorption. However, two systems at equilibrium with equivalent water saturations may have different $A_{ia}$ values due to differences in the water morphology. Water morphology depends on physical properties of system (e.g. grain size, soil texture, pore-size distribution, and wetting/drying cycles).[12,17] For example, a soil system containing several large blobs of water would have a small AWI compared to a system at an equivalent water saturation containing many small blobs. Contaminant vapor traveling through the latter system would be retained longer because it would be exposed to a greater interfacial area. To better understand how $A_{ia}$ varies, the processes controlling the precise water morphology need to be understood.

*Adsorption- and Capillary-Associated Air-Water Interfaces*

Water in a porous medium is retained primarily by two processes that combine to form $A_{ia}$: capillary processes and adsorption processes.[12] Capillary processes refer to water held between grains in pendular rings and pore throats as shown in Figure 1-1, A and B.[12,17] These individual rings and throats can either be connected to the bulk water, or trapped as disconnected units.[17] The pressure difference across the AWI affects the water morphology, and thus, the magnitude of $A_{ia}$. The pressure difference across the interface for a given pore throat is given by the Young-Laplace equation:

$$p_\alpha - p_\beta = \frac{2\gamma}{r} \qquad [1\text{-}2]$$

where $p_\alpha$ and $p_\beta$ are the internal and external pressures across the meniscus, $\gamma$ is the surface tension, and r is the radius. Smaller pore dimensions result in water being held by stronger capillary forces. Thus, small pores fill more readily and also require greater suction to drain. The second process, adsorption, refers to the thin films of polar water molecules attracted to the charged surfaces of mineral grains, shown in Figure 1-1, C.[12,17] The thickness of the thin-films is related to the number of water monolayers covering the mineral grains. At low water saturations associated with monolayer coverage, the AWI is expected to approximate the surface area of the porous medium.[4,11,17]

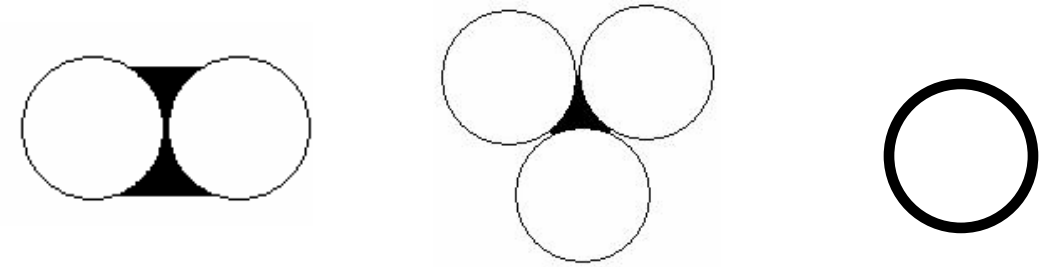

**A: Pendular rings** **B: Pore throats** **C: Thin films**

**Figure 1-1.** Processes by which water is retained in a soil column. A and B represent capillary process, while C is an adsorption process.[17]

*Air-Water Interfacial Area Trends*

Currently, two conceptual models describe the $A_{ia}$-water saturation ($S_w$) relationship. The first model, presented in 1991 by Gvirtzman and Roberts[18] using computer modeling, predicts a parabolic relationship with zero $A_{ia}$ at both $S_w$ extremes, and maximum $A_{ia}$ occurring at $S_w$ associated with maximum pendular ring formation (Figure 1-2). Later mathematical modeling by Reeves and Celia[19] supports this parabolic trend. The second model, presented in 1994 by Cary[20], predicts a nonlinear continually decreasing $A_{ia}$ trend with increasing $S_w$, and was later supported by Or and Tuller[21], and Silverstein and Fort.[22] The Cary model predicts maximum $A_{ia}$ to occur at low $S_w$, where a thin film of water on individual particles dominates retention. In 2002, Costanza-Robinson and Brusseau[12] reconciled the two conceptualizations by hypothesizing that the two groups were actually modeling different interfaces. The first focuses solely on capillary-associated AWI (i.e. pendular rings and pore throats), while the second concentrates more on adsorption processes (i.e. thin-films). Thus using experimental results, Costanza-Robinson and Brusseau[12] proposed a new relationship combining the two models with greatest $A_{ia}$ at low $S_w$, but dropping to zero for a completely dry media. Thin-films were hypothesized to dominate solute retention at low $S_w$, with capillary processes becoming more important for systems at higher $S_w$. Bryant and Johnson[17] were able to combine both models in their modeling work. They first examined how capillary-associated $A_{ia}$ is affected by water blob connectivity. However, by adding the thin-films of adsorbed water to their model, Bryant and Johnson were able to distinguish the relative importance of the two processes for varying $S_w$. At low $S_w$, they found thin film-associated $A_{ia}$ to be an order of magnitude larger than capillary-associated $A_{ia}$.[17]

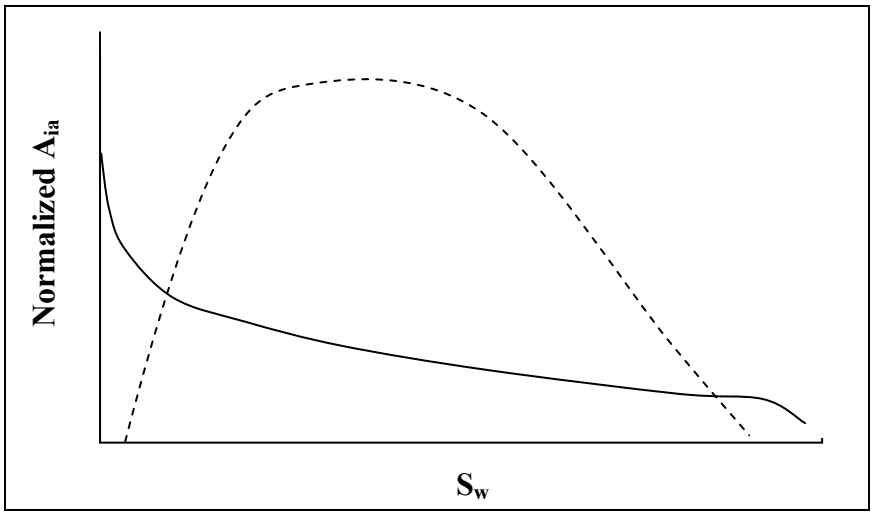


**Figure 1-2.** Different models proposed for $A_{ia}$-$S_w$ relationship. Dotted line represents models only accounting for capillary AWI (e.g. Gvirtzman and Roberts[18]). Solid line represents models accounting for capillary and thin-films of adsorbed water (e.g. Cary[20]).

The decision whether or not to consider the thin-films of adsorbed water as part of the total AWI depends upon the application. For example, because adsorbed-water films may contribute the majority of $A_{ia}$ in some environmental systems, neglecting thin films would lead to greatly underestimated contaminant retention. However, in other environmental applications, the thin films may be less relevant. For example, the larger surface area to volume ratio for thin films allows for faster mass transfer across the AWI. Kinetically, the thin films of absorbed water may not represent any mass transfer rate limitations. In practical remediation (e.g. SVE) scenarios, mass-transfer kinetics is often the limiting factor. Thus, the filled pores and thick water films are of primary importance, while the thin films have a smaller significance.[17] Provided the underlying assumptions of each model are understood, each offer unique benefits to the general understanding of the AWI.

*Measuring Air-Water Interfacial Areas*

Although the importance of the AWI is well documented, precise methods for measuring its areal extent have only recently been proposed.[10-12,23] In previous studies, reactive tracer tests have been the primary technique for measuring both air–water[4-5,24-26] and water–NAPL[4,24] interfaces. Interfacial tracer tests involve a tracer that is known to be retained primarily at the desired interface. The extent of the interface can, therefore, be estimated based on the magnitude of retention of the interfacial tracer. Because this method only requires monitoring at the inlet and outlet of the sweep zone, the methodology can be applied at the laboratory and field scales.[4]

Both gas-phase (used here) and aqueous-phase (surfactant) tracers have been used to measure $A_{ia}$. Kim et al.[27] used aqueous-phase interfacial tracer tests to measure $A_{ia}$ for a treated sand using sodium dodecylbenzene sulfonate (SDBS) as the interfacial tracer and sodium bromide as the nonreactive tracer. This study was then expanded to use a variety of compounds as reactive tracers and model contaminants, including four straight-chain alcohols, three chlorinated aromatic hydrocarbons, and two alkylbenzenes.[28] Results indicate a continually decreasing $A_{ia}$ with increasing $S_w$ like the Cary[20] modeling results. The aqueous-phase tests work best at higher $S_w$ when there is still a well-connected water network. Thus, the results from these studies can be used to complement the gas-phase tracer results performed at low $S_w$ (described below).[10] A variety of static method tests have also been used to measure $A_{ia}$ values in a variety of soil systems;[29-31] however, none of these methods are applicable at the field scale and thus, the dynamic interfacial tracer tests are preferred.

Recently, synchrotron X-ray computer-assisted microtomography (μ-CT) has been used to measure $A_{ia}$, capturing direct three-dimensional images of porous media on the scale of approximately 10 μm.[32-37] In 2002, Wildenschild et al.[32] used μ-CT to analyze pore geometry and distribution in a soil column. In 2004, Culligan et al.[28] imaged a glass bead system on imbibition and drainage loops. The image-derived $A_{ia}$ values agreed best with the parabolic relationship of Gvirtzman and Roberts[18] and Reeves and Celia.[19] At current image resolution, the surface roughness associated with the porous media remains invisible for microtomography. Thus, $A_{ia}$ measurements via μ-CT represent a smoothed approximation of the total AWI. In fact, Brusseau et al.[36] recently compared total $A_{ia}$ values (thin-film and capillary) for a single natural porous medium using gas-phase interfacial tracers and μ-CT. Gas-phase tracer derived $A_{ia}$ values approached the $N_2$/BET measured surface area, while μ-CT derived $A_{ia}$ values approached the smooth-sphere approximated area.[36]

*Gas-Phase Interfacial Tracers*

For the gas-phase interfacial tracer methodology, a nonreactive tracer (methane) and an interfacial tracer (decane vapor) are passed through the porous medium. The relative retardation of the interfacial tracer is used in Equation 1-1 to measure $A_{ia}$ of the system. Decane vapor is used as an interfacial tracer to maximize the relative importance of $R_{ia}$. With a high molecular mass and stronger dispersion forces, decane is less volatile and less soluble than methane, and thus more likely to adsorb at the AWI.[4,10] Because the tracer effectively probes the entire AWI, this methodology is hypothesized to measure both adsorption- and capillary-associated $A_{ia}$.[11-12] Figure 1-3 shows the pulse of

nonreactive tracer (methane) and reactive interfacial tracer (decane) passing through the soil column versus time. The relative retardation of decane to methane is used to calculate $A_{ia}$.

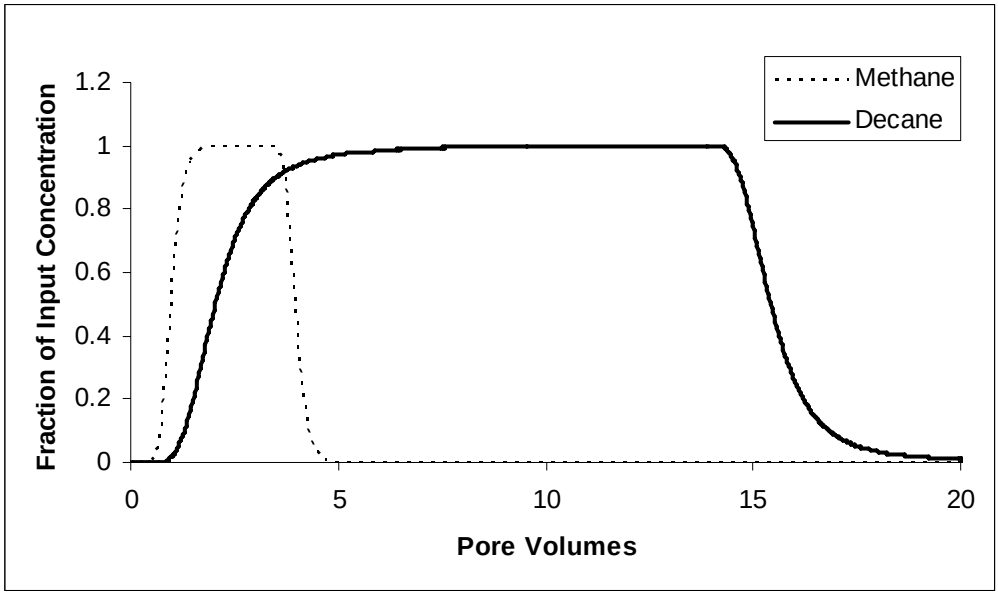


**Figure 1-3.** Representative breakthrough curves for a nonreactive tracer, methane, and a reactive tracer, decane.

Previous studies using gas-phase interfacial tracers to measure $A_{ia}$ support the trend of decreasing non-linear $A_{ia}$ values with increasing $S_w$, and thus are most likely measuring $A_{ia}$ due to both adsorption and capillary processes.[5,11-12,26] Comparisons among studies is often difficult because of different experimental conditions (e.g. flow rates, $S_w$, bulk densities) and porous media studied. However, using maximum measured $A_{ia}$ values across several studies, Costanza-Robinson and Brusseau[12] found that measured $A_{ia}$ values increased with increasing surface area, as expected.

*Objectives of this Study*

The first objective of this work was to compare the measured $A_{ia}$-$S_w$ relationship for two porous media systems: Vinton (fine sand with small amounts of silt and clay) and Granusil 7030 (fine sand). The two porous media have similar average grain size and smooth sphere-approximated surface areas, but differ in surface roughness as represented by $N_2$/BET surface areas of 3.33 and 0.56 $m^2/g$, respectively. The second objective was to use the measured $A_{ia}$ values to predict the retardation of the contaminant TCE through the same soil systems. These predicted retardation factors were compared to the measured values to evaluate the gas-phase interfacial tracer technique. Characterizing how $A_{ia}$ varies with different soil systems is critical for understanding and predicting contaminant transport in subsurface systems.

# II. METHODS

*General Theory*

The transport of organic vapors passing through a low-SOM soil system is retarded based upon its interaction with the solid-phase ($R_s$), water ($R_w$), and air-water interfacial ($R_{ia}$) domains. Thus, the retardation of a given contaminant, X, is given by

$$R^X = 1 + R_s + R_w + R_{ia} = 1 + \frac{\rho_b K_d^X}{\theta_a K_h^X} + \frac{\theta_w}{\theta_a K_h^X} + \frac{K_{ia}^X A_{ia}}{\theta_a} \qquad [2\text{-}1]$$

where $\rho_b$ refers to the bulk density ($g/cm^3$), $K_d$ is the saturated-phase sorption coefficient ($cm^3/g$), $K_h$ is the dimensionless Henry's Law coefficient (-), $K_{ia}$ is the air-water interfacial adsorption coefficient (cm), $\theta_a$ and $\theta_w$ are the volumetric air-filled porosity and water content, respectively (-), and $A_{ia}$ is the volume-normalized air-water interfacial area ($cm^{-1}$).

For a well-studied gas-phase solute, all of the physical and chemical constants in Equation 2-1 are known except for $A_{ia}$. The variables describing the porous medium or environmental system, such as bulk density and water content, can be easily measured. This study used the gas-phase interfacial tracer technique to estimate $A_{ia}$ values at varying water saturations, 3.9-23.4% $S_w$ for Vinton and 2.3-18.5% $S_w$ for Granusil 7030. All gas-phase solutes were custom-blended in a balance of nitrogen and stored in high-pressure gas cylinders (Advanced Specialty Gases, Reno, NV).

Methane (100 ppmV) was chosen as the non-reactive tracer because it experiences negligible retention in any of the domains in Equation 2-1, and thus, its retardation factor is assumed to be 1. Decane (2 ppmV) was used as the reactive tracer because it experiences little retention via the solid phase and bulk water, and 99% of its

retardation has been attributed to $R_{ia}$.[12] Due to its much lower saturation vapor pressure, it was used at a significantly lower concentration than methane to avoid condensation.[12] The retardation equation for decane can be approximated as

$$R^{decane} = 1 + \frac{K_{ia}^{X} A_{ia}}{\theta_a} \qquad [2\text{-}2]$$

Thus, once the retardation factor of decane is known in a given soil system, $A_{ia}$ can be estimated. Estimated $A_{ia}$ values were used to predict the retardation factor of the contaminant trichloroethylene (TCE) (100 ppmV) in Vinton and Granusil 7030. The predicted TCE retardation factors were then compared to the measured values to assess the efficacy of the gas-phase tracer method for measuring $A_{ia}$.

*Porous Media Properties*

Vinton, a fine sand with small amounts of silt (1.8%) and clay (1.2%) (University of Arizona Agriculture Center, Tucson, AZ), and Granusil 7030, a fine sand (Unimin Corporation, Emmett, Idaho), were chosen as the two porous media for this study after qualitative observations using scanning electron microscopy (Figure 2-1). Because the Vinton sand had visible organic matter, it was removed by heating in a muffle furnace at 500° C for 8 hours. The two media were chosen because they have a similar average grain size, but Vinton sand has significantly more surface roughness than Granusil 7030 as represented by the $N_2$/BET surface area (Table 2-1). Relevant physical properties of the two porous media are given in Table 2-1. A smooth-sphere approximation of the surface area, $S_a$, was calculated using the formula

$$S_a(cm^{-1}) = \frac{6(1-n)}{d_{50}} \qquad [2\text{-}3]$$

where $n$ is the porosity of the packed porous medium system (-), and $d_{50}$ is the average particle diameter (cm). Because this approximation assumes spherical grains with no surface roughness, the ratio of the $N_2$/BET surface area to $S_a$ yields a shape/roughness factor (SRF) for each media. Although $S_a$ is nearly identical for both media, Vinton, with a greater surface roughness, has a SRF of 349 compared to 52 for Granusil 7030.

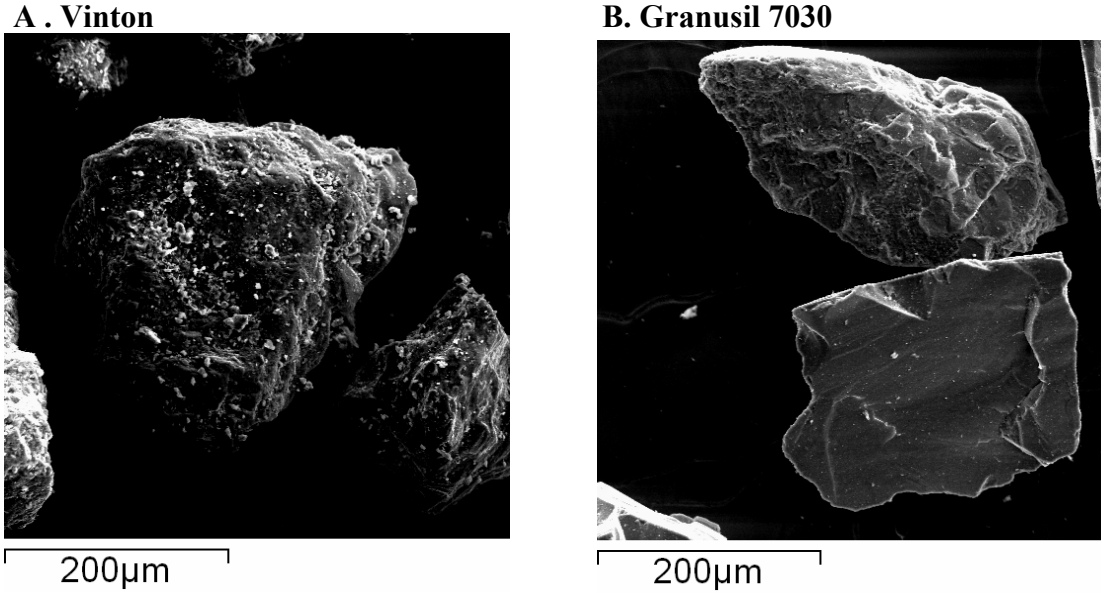


**Figure 2-1.** Scanning electron microscopy images of A) Vinton and B) Granusil 7030.

**Table 2-1.** Physical Properties of Porous Media

| **Parameter** | **Vinton** | **Granusil 7030** |
|---|---|---|
| Mean diameter, $d_{50}$ (mm) | 0.234 | 0.200 |
| Uniformity coefficient, U (-)[a] | 2.4 | 1.7 |
| $N_2$/BET surface area, SA ($cm^2/g$) [b] | 33,300 | 5,600 |
| $S_a$ ($cm^{-1}$)[c] | 169 | 162 |
| SRF (shape/roughness factor) (-)[d] | 349 | 52 |

[a] $U = d_{60} / d_{10}$

[b] Micrometrics, Inc. (Norcross, GA)

[c] $S_a$ was calculated under the smooth sphere approximation (Equation 2-3)

[d] $SRF = \frac{SA \times \rho_b}{S_a}$

*Column Preparation*

The porous medium was packed into a 25-cm long by 2.2-cm i.d. stainless steel column in 3-g aliquots. Tamping the column between aliquots helped ensure tight packing and achieve bulk densities similar to natural conditions. Stainless steel dispersion plates (~20-μm pores) were placed at each end to yield an even distribution of vapor across the column. Bed-support frits (2-μm pores) were also inserted on each end of the column to prevent soil grains from clogging the dispersion plates. Following the methodology of Kim et al.,[26] a small amount of water (~500 μL) was added to each end of the column, which was then sealed with stainless steel plugs. The column was placed in the oven at 150 °C for approximately 12 hours, allowing the water to vaporize and uniformly fill the column. The column cooled to room temperature, allowing the water to preferentially fill the small pores as it condensed. This methodology achieved relatively uniform water saturations with a reasonably realistic water morphology. This process was repeated until the desired water saturation was achieved.

*Equilibrium constants*

$K_D^{sat}$ refers to the equilibrium adsorption tendency of a solute to the solid phase from the water phase. Because $K_D^{sat}$ values are both solute and soil-specific, they need to either be measured or estimated for each contaminant/porous media combination. Costanza-Robinson's[4] measured $K_D^{sat}$ value of 0.014 $cm^3/g$ for TCE in Vinton was used for this study (Table 2-2). Decane, however, has a very low aqueous solubility, and could not be measured using conventional methods. Unfortunately, there are few estimation methods in the literature, and none have focused on straight chain alkanes in

soils with low SOM. There are several methods for estimating organic carbon or organic matter partitioning constants, from which $K_D^{sat}$ values can be deduced using the following relationships:

$$K_D^{sat} = K_{OC} f_{OC} \qquad [2\text{-}4]$$

$$K_D^{sat} = 1.724 K_{OM} f_{OC} \qquad [2\text{-}5]$$

where $K_{OC}$ and $K_{OM}$ refer to the organic carbon and organic matter partitioning constants ($cm^3/g$), respectively, and $f_{OC}$ is the fraction of organic matter. For both Vinton[4,12] and Granusil 7030[11] soils, $f_{OC}$ was estimated at 0.0001.

Without a $K_{OC}$ estimation specific to decane, four different methods were averaged. Lyman[38] developed two sets of semi-empirical equations defining the relationship between $K_{OC}$ and solubility:

$$\log K_{OC} = -0.55 \log S + 3.64 \qquad [2\text{-}6]$$

$$\log K_{OC} = -0.557 \log S + 4.277 \qquad [2\text{-}7]$$

where S refers to solubility (mg/L and μmol/L, respectively). Equation 2-6 was defined using 106 compounds representing a variety of compound classes, while Equation 2-7 used 15 hydrocarbons. Using octanol-water portioning constants ($K_{ow}$) Lyman[38] and Schwarzenbach et al.[39] developed the following relationships using 45 and 34 compounds, respectively:

$$\log K_{OC} = 0.54 \log K_{OW} + 1.377 \qquad [2\text{-}8]$$

$$\log K_{OM} = 0.82 \log K_{OW} + 0.14 \qquad [2\text{-}9]$$

Using Equations 2-6 through 2-9, an average $K_D^{sat}$ value of 2.9 ± 1.1 $cm^3/g$ was obtained for decane, which agreed with the estimated value used by Costanza-Robinson.[4] For

TCE, an average value of 0.02 ± 0.01 $cm^3/g$ was derived, which agreed favorably with 0.014 $cm^3/g$, measured experimentally by Costanza-Robinson[4] as listed in Table 2-2. The same equilibrium constants were used for solutes in Granusil 7030 experiments because both media are silica sands with negligible SOM.[11]

**Table 2-2.** Physicochemical Properties of Gas-Phase Solutes[a]

| | **Methane** | **Decane** | **TCE** |
|---|---|---|---|
| $K_D^{sat}$ ($cm^3/g$) | NA | 2.9[b] | 0.014[c] |
| $K_h$ (-) | 27[d] | 264[d] | 0.367[c] |
| $K_{ia}$ ($cm \times 10^{-5}$) | NA | 22.4[e] | 2.64[e] |

[a] Values at 25 °C, 1 atm
[b] Estimated in text
[c] Measured by Costanza-Robinson[4]
[d] Estimated by Schwarzenbach et al.[39]
[e] Measured by Hoff et al. 1993[8]

Table 2-2 also presents equilibrium constants for Henry's law and interfacial adsorption. Henry's law constant, $K_h$ gives the equilibrium distribution of solute between the soil-gas and bulk water. A higher value of $K_h$ corresponds to decreased dissolution capacity to the bulk water. The air-water interfacial adsorption coefficient, $K_{ia}$, describes the equilibrium concentration of a contaminant at the air-water interface relative to its gas-phase concentration, with a greater value corresponding to increased adsorption.

*Gas-Phase Miscible Displacement Experiments*

The gas-phase miscible displacement experimental setup is shown in Figure 2-2. Stainless steel tubing (1/8") carried all gases, and was washed with methanol to remove any residual oil that could retain organic contaminants. During an experiment, gas-phase solutes passed through 500-mL glass humidifier bottles (Pyrex, Mexico) to avoid

evaporation of the water from the porous medium. Separate humidifier bottles were used for the tracers/TCE and the carrier ($N_2$) to prevent cross contamination and were connected to the gas lines using PTFE connectors (Omnifit, England). Gas flow rates were controlled through the use of electronic pressure controllers (MKS Type 640A with a 247D four-channel readout, Wilmington, MA) and verified at the outlet using a digital flowmeter. Inlet pressure in the system was minimized (<3 psi) to reduce gas expansion along the axis of flow. Swagelok stainless steel three-way valves were used to switch between gases and to switch between the soil column and bypass line. The dead volume of the system was 1.60 mL, which, at 1.8% of the column volume, was below the recommended 10%.[4] The column effluent was monitored using a flame ionization detector (FID) on a HP 5890 Series II gas chromatograph. Flow rates to the FID were 400 mL/min for air and 30 mL/min for $H_2$, and the FID temperature was 350 °C. The analog voltage output was routed to a Dataq 158U A to D converter module (Dataq Instruments, Akron, Ohio), and the plot of voltage versus time, a breakthrough curve, was captured using Windaq Acquisition and Windaq Waveform Browser software (Dataq Instruments Version 3.16).

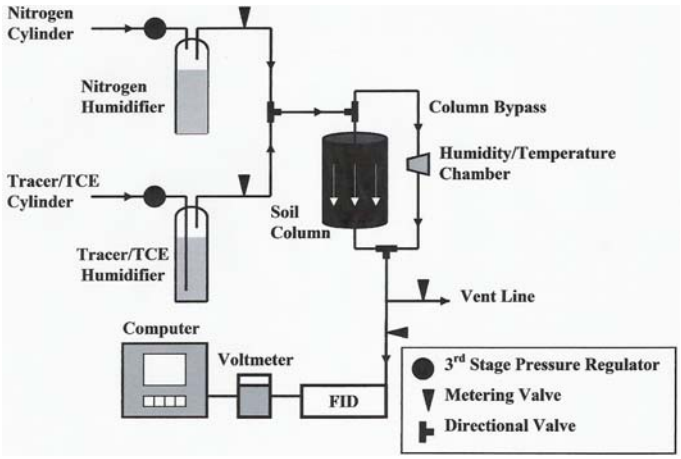


**Figure 2-2**. Schematic of Gas-Phase Miscible Displacement System.[4]

A nominal volumetric flux of 20 mL/min was chosen for all column experiments to represent typical SVE conditions.[2-3] $N_2$ carrier was used to establish a baseline FID voltage. Flow was switched to tracer/TCE, and the Windaq software began recording the signal. The input pulse was continued until a steady voltage ($V_f$) was achieved, indicating equilibrium partitioning had been achieved. Flow was switched back to $N_2$ to elute the tracer/TCE retained in the column. All gas-phase miscible displacement experiments were performed in at least triplicate. Sorption to the stainless steel system was measured by running experiments on an empty column.

Seven gas-phase miscible displacement experiments were run for each gas-phase solute, at 3.9-23.4% $S_w$ for Vinton and 2.3-18.5% $S_w$ for Granusil 7030. Experimental conditions for Vinton and Granusil 7030 experiments are listed in Tables 2-3 and 2-4, respectively. Two soil columns (A and B) were used for each media to examine whether media packing affected results.

**Table 2-3. Column Specifications for Vinton Experiments**

| Saturation (%) | Column | Bulk Density ($g/cm^3$) | Porosity (–) | $\theta_a$ (–) | $\theta_w$ (–) | $S_w/S_m$ (-) |
|---|---|---|---|---|---|---|
| 3.9 | A | 1.77 | 0.341 | 0.328 | 0.013 | 7.6 |
| 5.0 | B | 1.78 | 0.339 | 0.322 | 0.017 | 9.7 |
| 7.0 | A | 1.77 | 0.342 | 0.318 | 0.024 | 13.6 |
| 9.7 | B | 1.78 | 0.338 | 0.305 | 0.033 | 18.8 |
| 14.6 | A | 1.77 | 0.343 | 0.293 | 0.050 | 28.4 |
| 17.5 | B | 1.78 | 0.338 | 0.279 | 0.059 | 34.0 |
| 23.4 | A | 1.76 | 0.345 | 0.264 | 0.081 | 45.5 |

**Table 2-4. Column Specifications for Granusil 7030 Experiments**

| Saturation (%) | Column | Bulk Density ($g/cm^3$) | Porosity (–) | $\theta_a$ (–) | $\theta_w$ (–) | $S_w/S_m$ (-) |
|---|---|---|---|---|---|---|
| 2.3 | B | 1.49 | 0.448 | 0.438 | 0.010 | 41.8 |
| 4.9 | A | 1.48 | 0.449 | 0.427 | 0.022 | 89.0 |
| 7.7 | B | 1.51 | 0.439 | 0.405 | 0.034 | 140 |
| 9.2 | A | 1.49 | 0.448 | 0.407 | 0.041 | 167 |
| 10.0 | B | 1.51 | 0.439 | 0.395 | 0.044 | 182 |
| 14.5 | B | 1.51 | 0.439 | 0.375 | 0.064 | 263 |
| 18.5 | B | 1.51 | 0.439 | 0.358 | 0.081 | 336 |

The degree to which the mineral grains are water-solvated can be quantified by comparison of actual $S_w$ to the $S_w$ required for monolayer water coverage, $S_m$, which is calculated as

$$S_m = \frac{\rho_s \times SA \times \rho_b}{\rho_w \times n} \qquad [2\text{-}10]$$

where $\rho_s$ is the area density of water at monolayer conditions ( $\rho_s = 2.9 \times 10^{-4}$ g/m$^2$),[11] SA is the $N_2$/BET surface area ($m^2/g$), $\rho_b$ is the bulk density of the media ($g/cm^3$), $\rho_w$ is the volume density of water ($g/cm^3$), and *n* is the porosity. Monolayer coverage is achieved at 0.52% saturation for Vinton and 0.055% saturation for Granusil 7030. The number of effective monolayers is then defined as the ratio: $S_w/S_m$ (Tables 2-3 and 2-4). Because Vinton has a larger surface area than Granusil 7030, a given $S_w$ will represent fewer equivalent monolayers for Vinton.

*Data Analysis*

The FID signal was plotted versus time at 0.5-s intervals to create a breakthrough curve for each experiment. Temporal comparative moments analysis was used to

calculate the retardation factors for decane and TCE in each experiment. The 0th moment, $M_0$, represents the area under a curve, and is defined as

$$M_0 = \int_0^t c \cdot dt \qquad [2\text{-}11]$$

Thus, the 0th moment measures the total mass recovered at the column outlet. Comparison to the known input pulse provides an estimate of the percent mass recovered.

The 1st normalized moment, $M_1$, of each curve is a measure of how long it takes for the center-of-mass to pass through the column. Correcting for the length of the input pulse yields a measure of the travel time ($T_{travel}$).

$$T_{travel} = M_1 - (0.5 \times pulse) = \frac{\int_0^t ct \cdot dt}{\int_0^t c \cdot dt} - (0.5 \times pulse) \qquad [2\text{-}12]$$

Travel times for decane and TCE relative to methane are used to calculate retardation factors (R):

$$R_{decane/TCE} = \frac{T_{decane/TCE}}{T_{methane}} \qquad [2\text{-}13]$$

Using Equation 2-1, the measured retardation factor for decane is used to determine $A_{ia}$ for a given soil column. Once $A_{ia}$ is known for a given system, Equation 2-1 was used to predict R for TCE, which was then compared the measured value.

*CXTFIT Modeling*

CXTFIT 2.1[40] was used to model flows and estimate transport parameters based on the standard convection-dispersion equation (CDE). Assuming steady-state one-

dimensional flow under equilibrium conditions with no degradation, the CDE can be written as:

$$\frac{\partial C}{\partial t} = -v\frac{\partial C}{\partial x} + D\frac{\partial^2 C}{\partial x^2} \qquad [2\text{-}14]$$

where C is the normalized solute concentration (-), t represents time (T), $v$ represents the average linear velocity ($v = \frac{Q}{nA}$, where Q is the Darcy flux, $n$ is porosity, and $A$ is the column cross-sectional area) (L/T), $x$ represents position along the flow axis (L), and D is the dispersion coefficient ($L^2/T$). CXTFIT fits the CDE to the experimental breakthrough curves by using a nonlinear least-squares parameter optimization. The measured retardation factor and known tracer/TCE input pulse are fixed input parameters, while the program optimizes for υ and D.[40] From the fitted values, a Peclet number, P, is calculated according to the formula

$$P = \frac{L v}{D} \qquad [2\text{-}15]$$

The Peclet number is a measure of the relative significance of advective to dispersive processes experienced by a solute. Thus, higher values for P correspond to more ideal flow for a particular experiment.

# III. RESULTS

Gas-phase miscible displacement experiments were completed for each gas-phase solute in at least triplicate at seven water saturations ($S_w$) for both Vinton and Granusil 7030. A single representative replicate is shown in all figures. Breakthrough curves for each experiment yielded a measure of the travel time for each gas-phase solute, from which retardation factors (R) were derived and, for decane, used to calculate $A_{ia}$.

The empty-column experiment, used to measure retardation due to sorption to the stainless steel apparatus, yielded values of $R_{ss} = 3.4$ for decane and $R_{ss} = 0.1$ for TCE, as shown in Figure 3-1. These values are higher than $R_{ss} = 0.9$ for decane and $R_{ss} = 0.09$ for TCE, measured by Costanza-Robinson,[4] possibly due to ambient temperature differences. $R_{ss}$ values were subtracted from the measured retardation factors in subsequent experiments to yield a corrected retardation factor, R', according to the formula

$$R' = R - R_{ss} = 1 + R_s + R_w + R_{ia} \qquad [3\text{-}1]$$

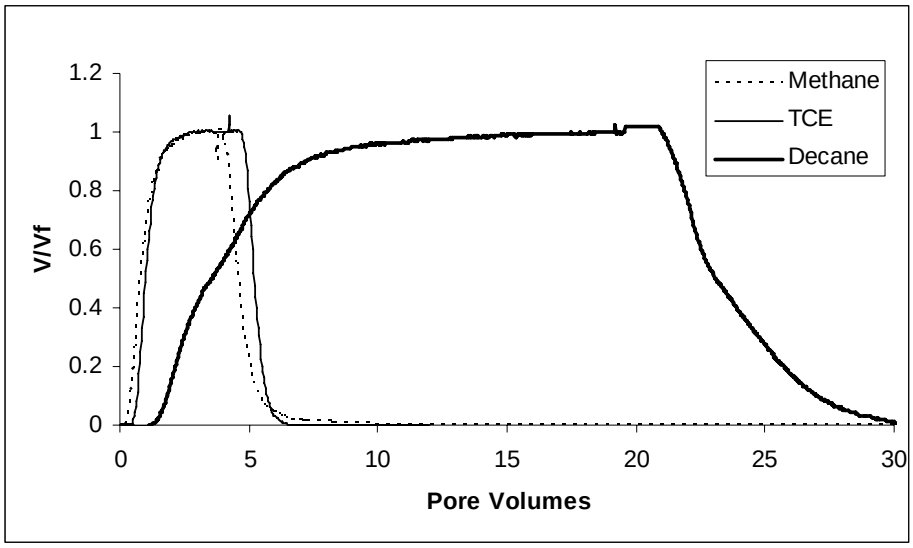


**Figure 3-1.** Decane and TCE sorption to stainless steel ($R_{ss} = 3.4$ for decane, $R_{ss} = 0.1$ for TCE.

*Vinton Breakthrough Curves*

Representative methane arrival and elution waves are shown in Figure 3-2. As expected, methane travel times generally decreased with increasing $S_w$ because the air-filled porosity decreased. This is shown in Figure 3-2 with experiments at higher $S_w$ shifted to the left.

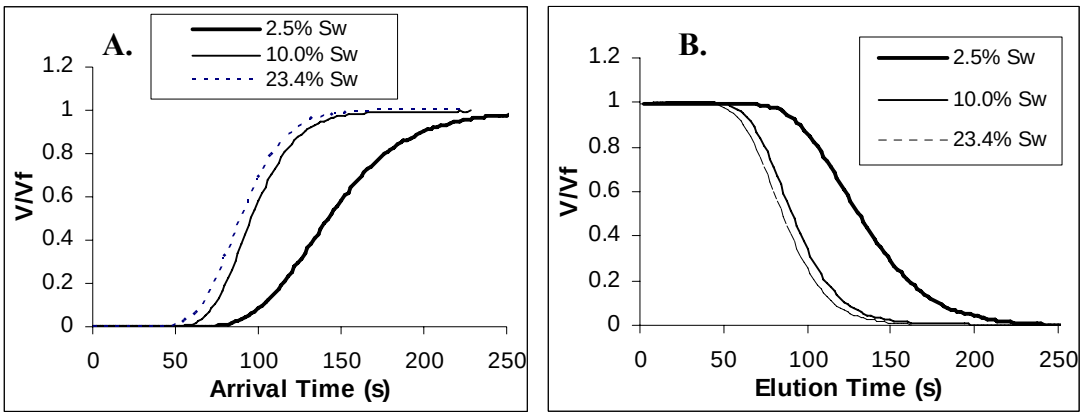


**Figure 3-2.** Representative methane breakthrough curves for Vinton experiments. A) Arrival wave; B) Elution wave.

As shown in Figure 3-3, the decane breakthrough curves also had decreased travel time corresponding with increased $S_w$. Pore volumes are used for the x-axis for a normalization and comparison between experiments. The experiments at the three lowest $S_w$ (i.e. 3.9%, 5.0%, and 7.0% $S_w$) are shifted to the right for both arrival and elution waves. Furthermore, the decane arrival and elution waves have a large degree of tailing, a characteristic not observed in the methane experiments.

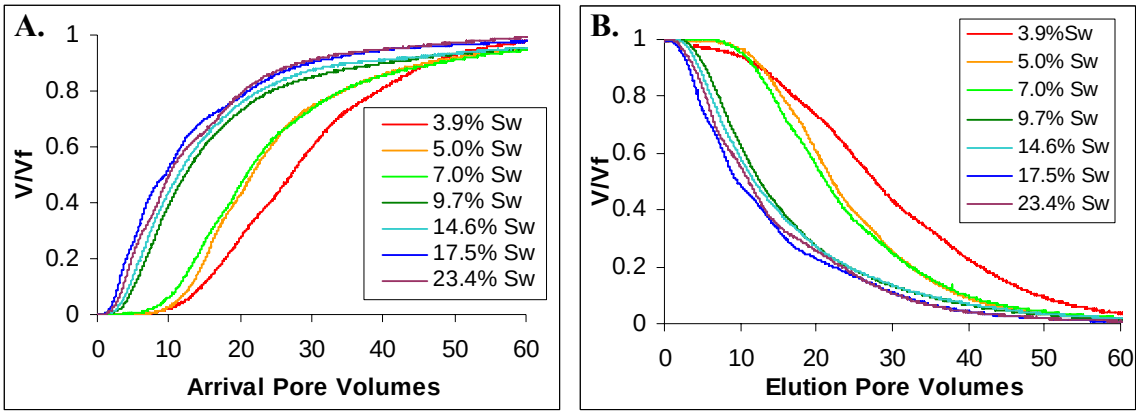


**Figure 3-3.** Representative decane breakthrough curves for Vinton experiments. A) Arrival wave; B) Elution wave.

TCE experiments were not conducted at 3.9% $S_w$ because mineral grain adsorption was expected to significantly affect retardation.[11] At this $S_w$, $A_{ia}$ values would be expected to be an overestimation, and the predicted retardation factors for TCE would not match the measured values. The retention trend exhibited by the breakthrough curves in Figure 3-4 for TCE was more complicated than that of methane or decane. Rather than a constant trend with $S_w$, the lowest retention was measured at 7.5% $S_w$ and increased at both lower and higher $S_w$. Unlike methane or decane, travel times for TCE generally increased with increasing $S_w$.

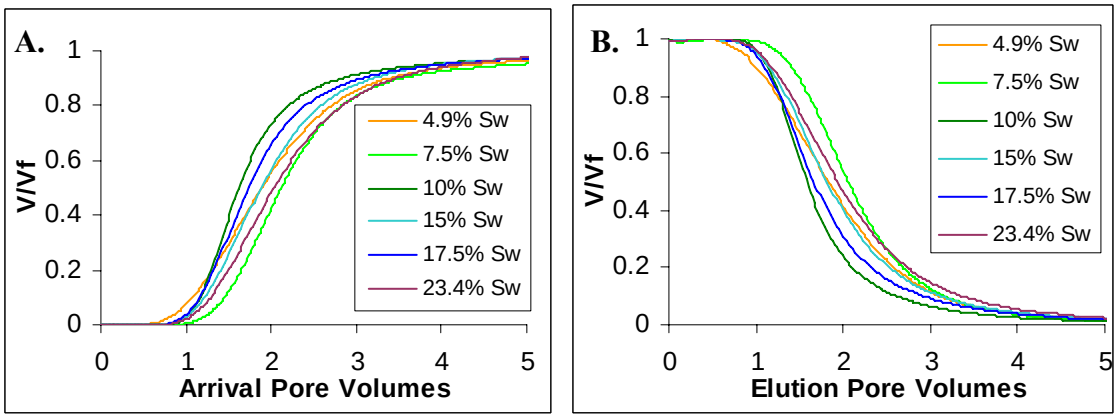


**Figure 3-4.** Representative TCE breakthrough curves for Vinton experiments. A) Arrival wave; B) Elution wave.

*Granusil 7030 Breakthrough Curves*

Representative methane arrival and elution waves are shown in Figure 3-5. As in the Vinton experiments, the methane travel times for Granusil 7030 generally decreased with increasing $S_w$ as the air-filled porosity decreased exhibited by shifting the left in Figure 3-5.

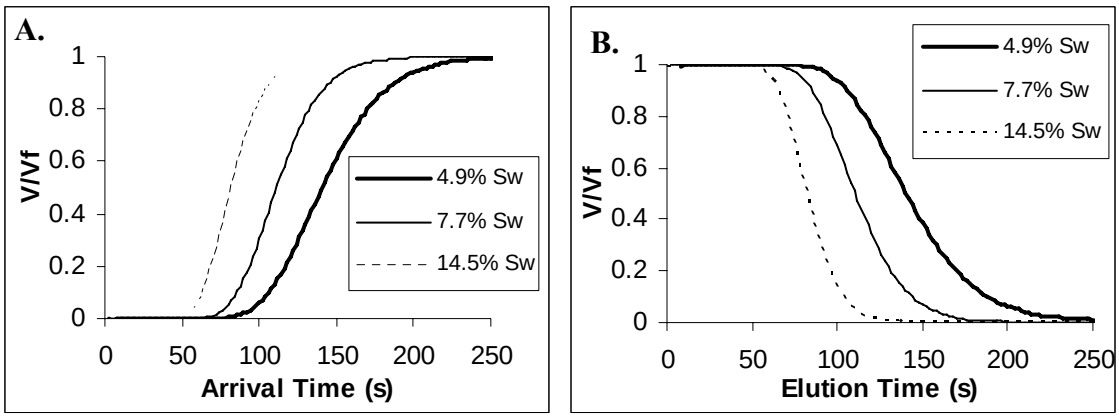


**Figure 3-5.** Representative methane breakthrough curves for Granusil 7030 experiments. A) Arrival wave; B) Elution wave.

Representative breakthrough curves for decane arrival and elution waves are shown in Figure 3-6. As with Vinton, experiments at lower $S_w$ are shifted to the right indicating increased adsorption. Like decane experiments for Vinton, the decane breakthrough curves for Granusil 7030 have a larger degree of tailing than for methane or TCE.

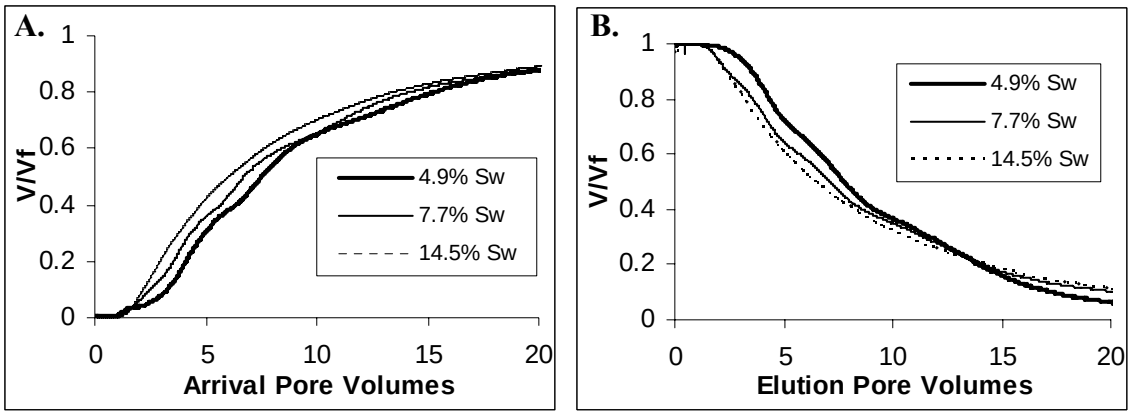


**Figure 3-6.** Representative decane breakthrough curves for Granusil 7030 experiments. A) Arrival wave; B) Elution wave.

Representative breakthrough curves for TCE experiments are shown in Figure 3-7. As with Vinton, the general trend is more complicated than the trend for methane and decane. Most experiments had similar travel times as shown by the overlap of many of the curves. The experiments at greater $S_w$ do not have decreased travel time as with methane and TCE. In fact, the experiments at the two greatest $S_w$ are shifted to the right, indicating increased retention.

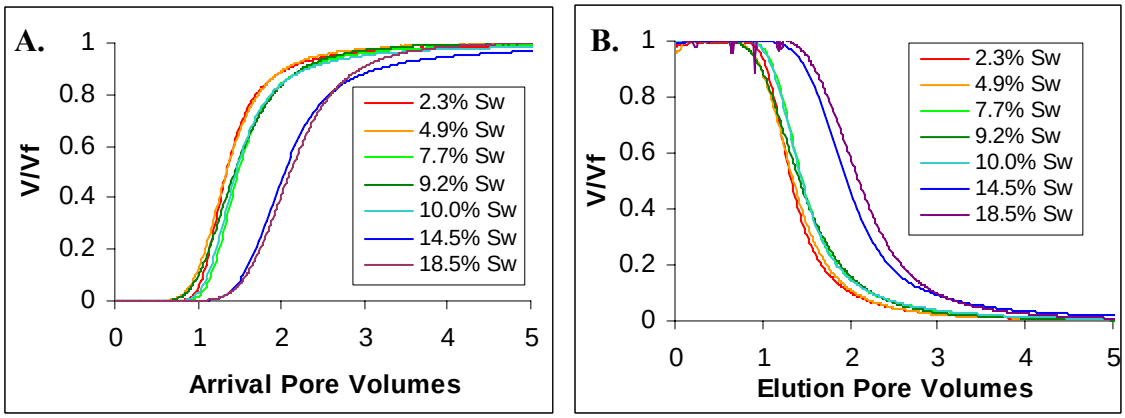


**Figure 3-7.** Representative TCE breakthrough curves for Granusil 7030 experiments. A) Arrival wave; B) Elution wave.

*Vinton Recoveries and Retardation Factors*

Recoveries for Vinton experiments were 99%-100% for methane, 96%-100% for decane, and 98%-100% for TCE. Lowest percent recovery and greatest variability between replicate experiments was observed at the two lowest saturations. At 5.0% $S_w$, the number of effective monolayers is 9.7 (Table 2-3) and mineral grain absorption may be affecting retention and, consequently, percent recovery. Thus, for Vinton, 5.0% $S_w$ may be the minimum for which decane is an effective interfacial tracer.

As shown in Figure 3-8, decane retardation factors are significantly greater than those for TCE as a result of its larger interfacial adsorption coefficient. Retardation factors for decane decreased with increasing $S_w$. Retardation factors for TCE were generally constant over the range of $S_w$ studied, achieving a minimum at 9.7% $S_w$.

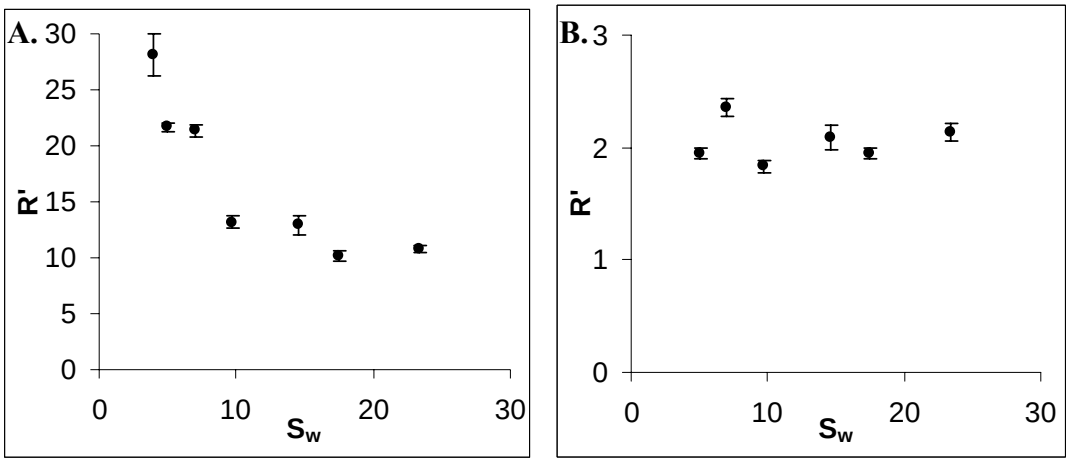


**Figure 3-8.** Decane and TCE retardation factors for Vinton experiments. Y-error bars represent one standard deviation. A) Decane; B) TCE.

The percent contributions of each retention domain to the total retardation of decane and TCE are graphed in Figures 3-9 and 3-10, respectively. Decane is a relatively ideal interfacial tracer because over 99% of its retardation is due to the AWI, with little

dissolution into the bulk water or sorption to the solid phase. On the other hand, the AWI adsorption is not always the main source of retardation for TCE. At low $S_w$, sorption to the solid phase is an important contributor, while at higher $S_w$ dissolution into bulk water dominates.

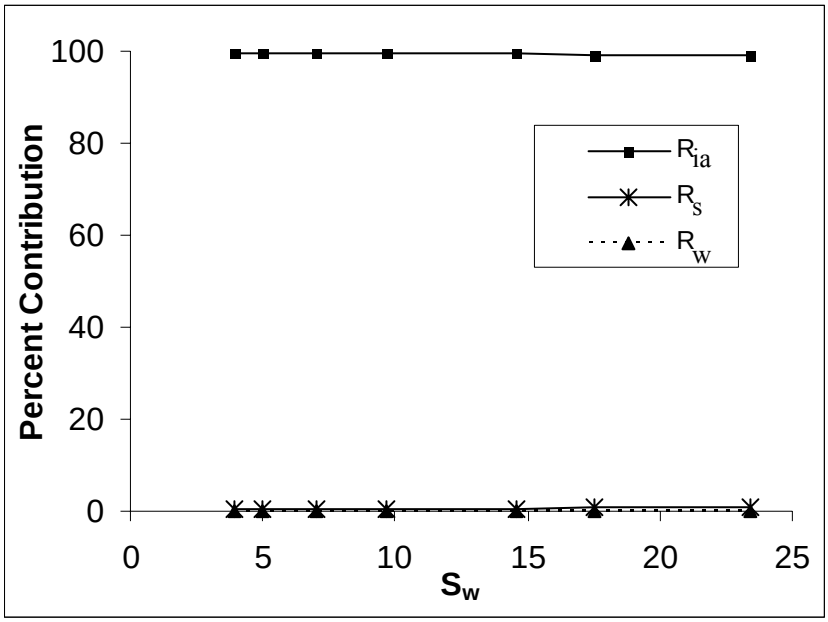


**Figure 3-9.** Domain contributions to the decane retardation factor for Vinton experiments.

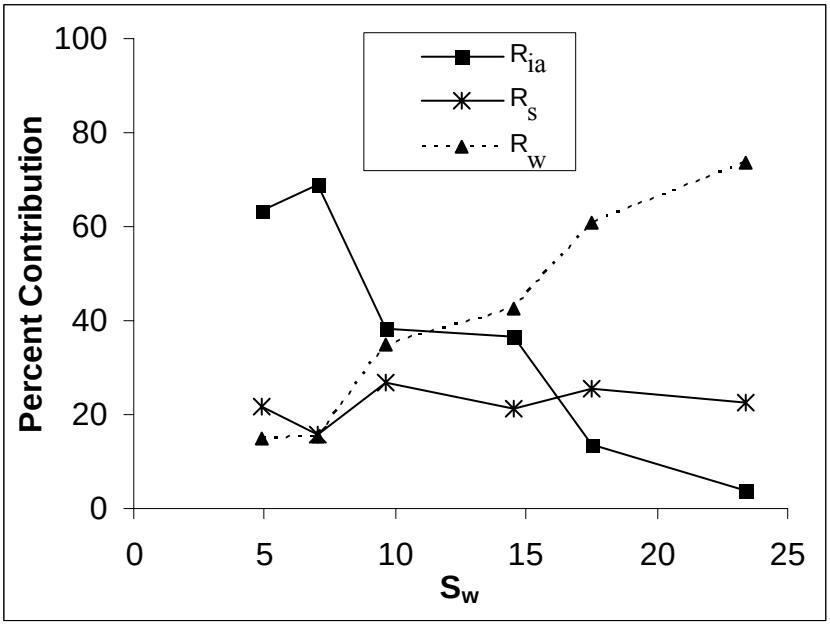


**Figure 3-10.** Domain contributions to the TCE retardation factor for Vinton experiments.

*Granusil 7030 Recoveries and Retardation Factors*

Recoveries for Granusil 7030 experiments were 99%-100% for methane, 97%-102% for decane, and 99%-100% for TCE. As for Vinton experiments, the standard deviation for recoveries was greatest at lowest $S_w$, suggesting that there may be some mineral grain adsorption. However, mineral grain adsorption is less likely for Granusil 7030 than for Vinton because at 2.3% $S_w$, the number of effective monolayers for Granusil 7030 is 41.8 (Table 2-4).

Decane and TCE retardation factors for Granusil 7030 experiments are shown in Figure 3-11. As expected, retardation factors for Granusil 7030 experiments are lower than those for Vinton experiments. As with Vinton, decane retardation was greater than TCE for all $S_w$. The greatest retardation for decane occurred at 2.3% $S_w$, and was otherwise relatively constant. The experiment at 4.9% $S_w$ had a smaller retardation factor than expected. However, the methane travel time for this experiment was also greater than expected. A smaller methane travel time would have led to a greater retardation factor for decane. TCE experiments were also relatively constant at most $S_w$, but reached a maximum at increased $S_w$, where dissolution into bulk water becomes an important contributor.

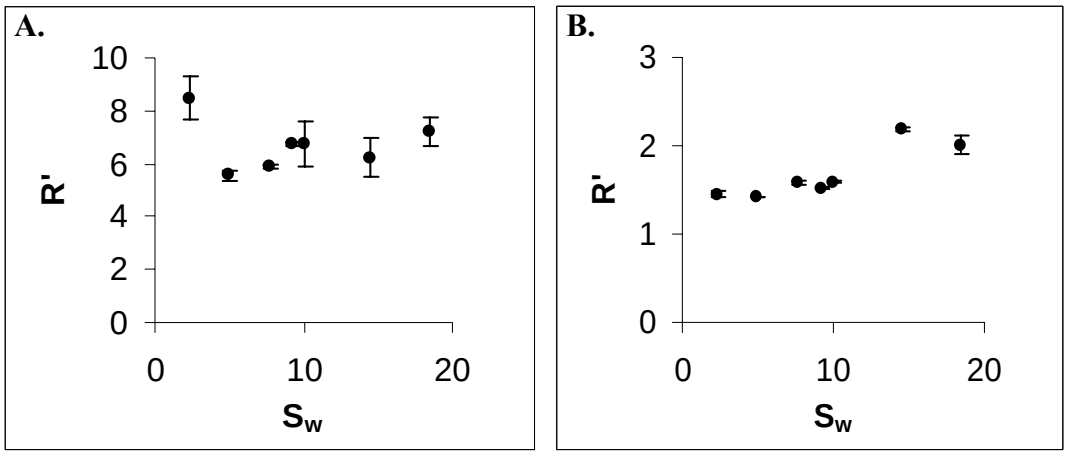


**Figure 3-11.** Decane and TCE retardation factors for Granusil 7030 experiments. Y-error bars represent one standard deviation. A) Decane; B) TCE.

The percent contributions of each retention domain to the total retardation of decane and TCE are shown in Figures 3-12 and 3-13, respectively. As with Vinton, over 99% of decane retardation is attributed to adsorption at the AWI. However, for TCE, adsorption to the solid phase and dissolution in water are also important contributors. However, the latter two alone would predict steadily increasing retardation with $S_w$. Instead, retardation factors for TCE remain relatively constant, and interfacial accumulation contributes 57% of observed retention at the lowest $S_w$ studied.

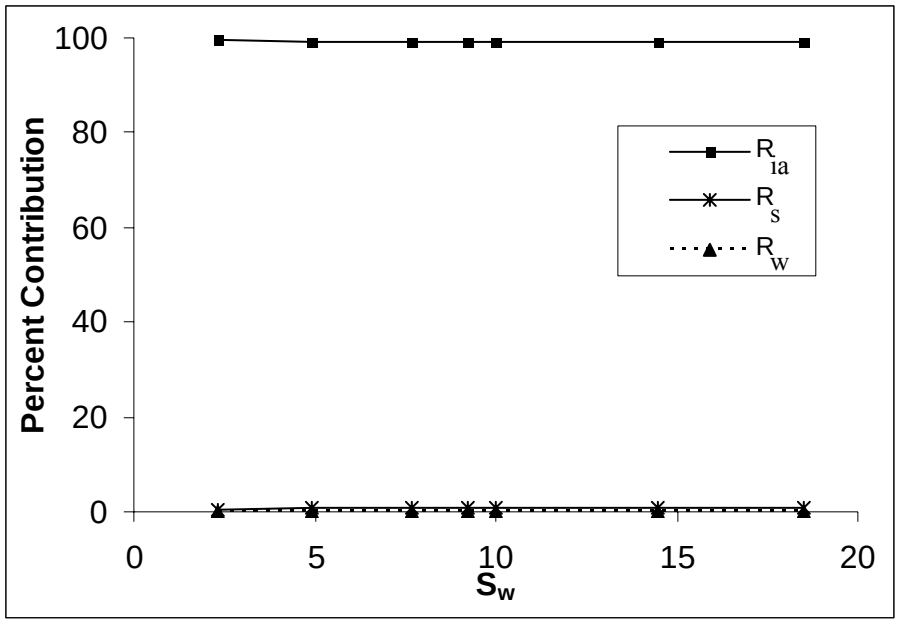


**Figure 3-12.** Domain contributions to the total decane retardation factor for Granusil 7030 experiments.

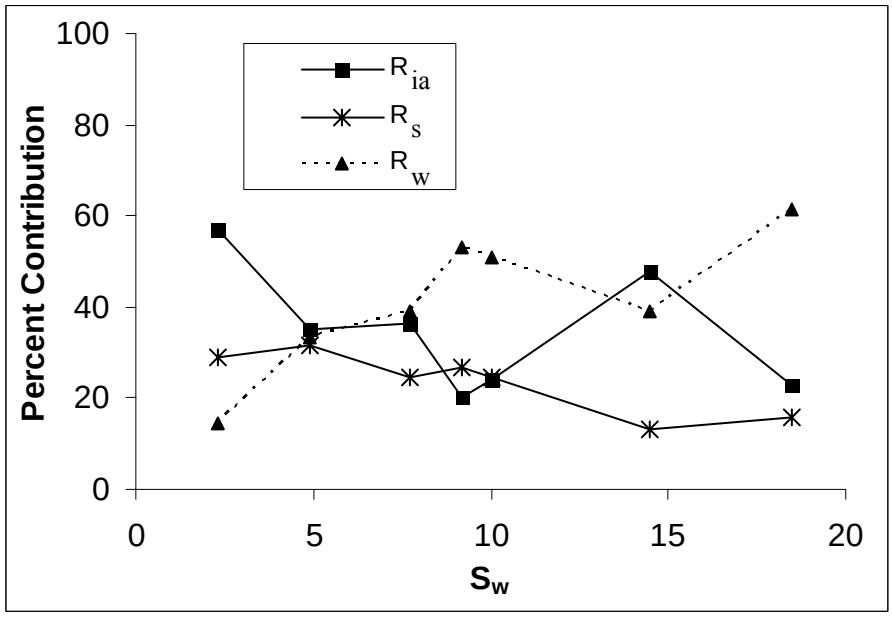


**Figure 3-13.** Domain contributions to the total TCE retardation factor for Granusil 7030 experiments.

*Air-Water Interfacial Areas*

Using the retardation factors measured for decane, $A_{ia}$ values were derived for all experiments. The observed $A_{ia}$-$S_w$ relationships for both media are shown in Figure 3-14. As expected, the interfacial areas decrease with increasing saturation. For Vinton, the maximum interfacial area occurred at 3.9% saturation and was 39,900 $cm^{-1}$. This value is less than the measured $N_2$/BET surface area (~59,000 $cm^{-1}$), and thus is a reasonable measurement. The maximum $A_{ia}$ value for Granusil 7030 was 14,500 $cm^{-1}$, and occurred at 2.3% saturation. Because this value is greater than the measured $N_2$/BET surface area (8400 $cm^{-1}$), it is not likely to be an accurate value for $A_{ia}$. Furthermore, the number of effective monolayers at 2.3% $S_w$ is 41.8 (Table 2-4), and thus, mineral grain adsorption is most likely not the explanation. One possible explanation is error in the interfacial adsorption coefficient, $K_{ia}$, used for decane in Equation 2-1. This topic will be explored later in Chapter IV.

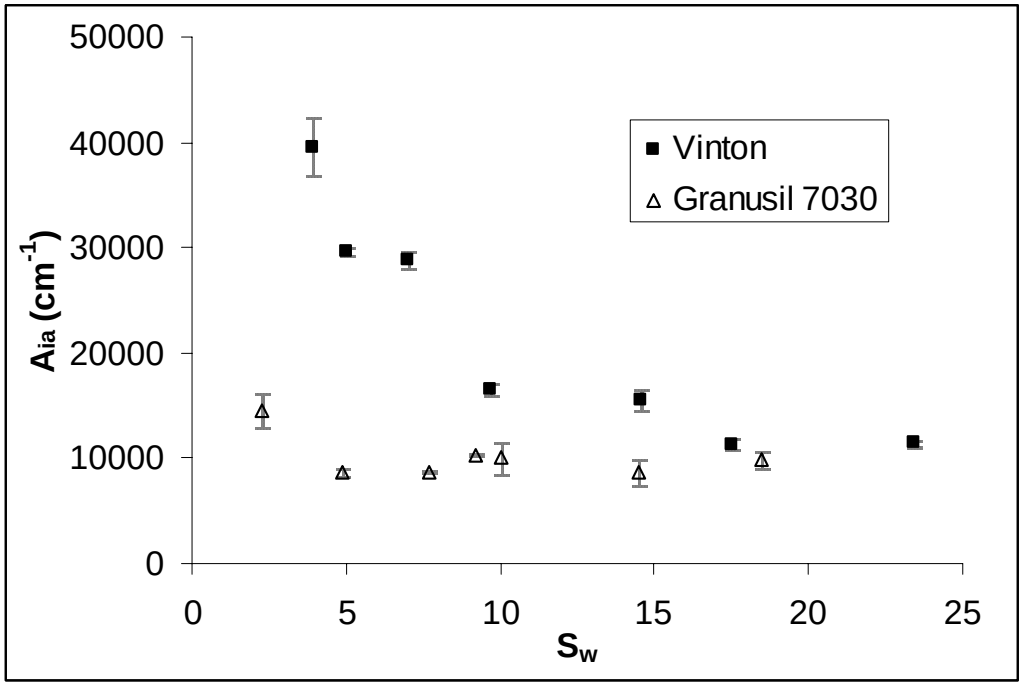


**Figure 3-14.** Measured $A_{ia}$ – $S_w$ relationship for Vinton and Granusil 7030. Y-error bars represent one standard deviation.

*TCE Predicted Retardation Factors*

Retardation factors for TCE were predicted using the measured $A_{ia}$ values obtained with decane and Equation 2-1. The predicted values are compared to the measured values for Vinton and Granusil 7030 in Figures 3-15 and 3-16. For both media, the predicted retardation factors follow the same general trend as the measured values; however, the predicted values are about 1.5 times measured values.

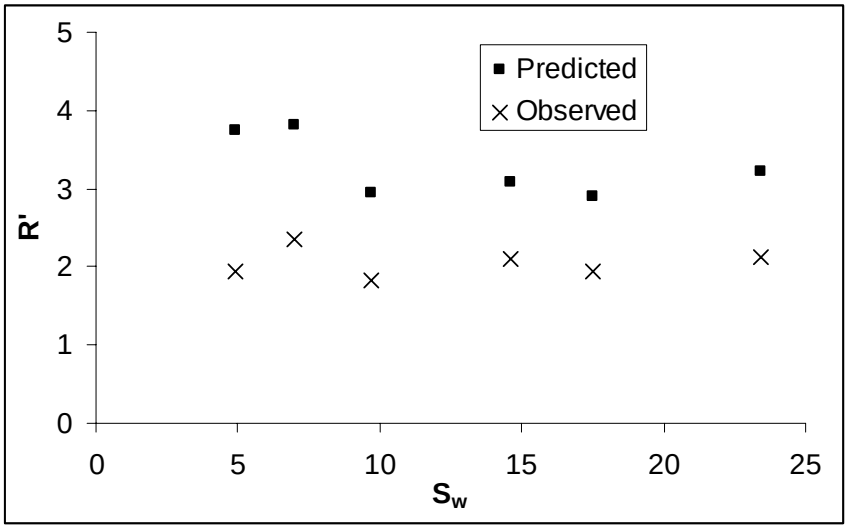


**Figure 3-15.** Comparison of predicted versus measured TCE retardation factors for Vinton.

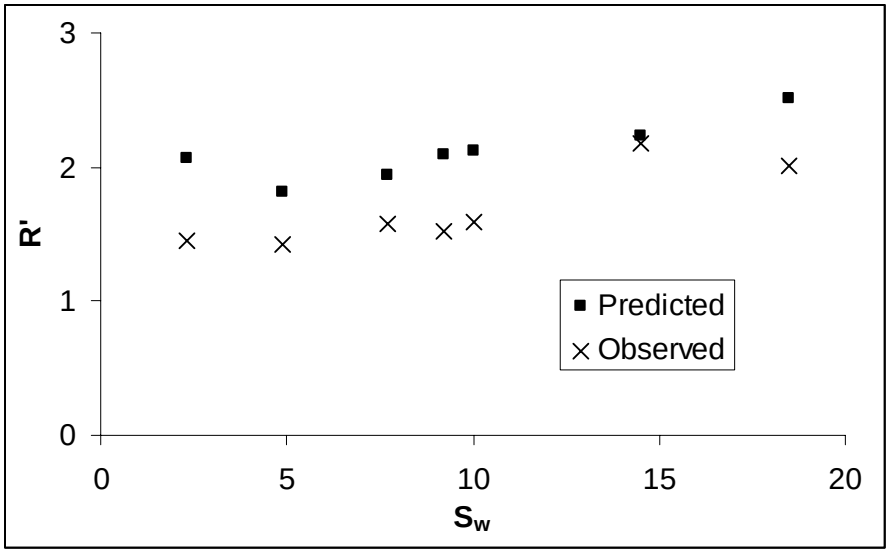


**Figure 3-16.** Comparison of predicted versus measured TCE retardation factors for Granusil 7030.

*CXTFIT Modeling Results*

Breakthrough curves were fitted using the computer program CXTFIT 2.1. Fitted curves not matching the original breakthrough curves were indications of experimental error (e.g. impurities, changing flow rates), and these experiments were repeated. As shown by representative breakthrough curves in Figure 3-17, fitted curves matched the observed data closely for all gas-phase solute experiments Optimized linear velocities (ν), dispersion coefficients (D), and Peclet numbers (P) are shown for Vinton and Granusil 7030 in Figures 3-18 and 3-19, respectively. The raw data are provided in the Appendix. For most experiments, ν increased with increasing $S_w$ because the air-filled porosity decreased while the volumetric flux was held constant. One notable exception is at 18.5% $S_w$ for Granusil 7030. For decane and TCE, D generally increased with increasing $S_w$, except for the experiment at 18.5% $S_w$ for Granusil 7030. For methane, D was relatively constant compared to the other gas-phase solutes. Because methane has the shortest residence time and least dispersion, it has the highest P for a given $S_w$. In contrast, decane has the largest values for D by at least one order of magnitude, and thus, lowest P values. For methane experiments, P remained constant for most $S_w$. Because of increasing D and decreasing ν, P generally decreased for all decane experiments. For TCE, P remained relatively constant, with a slight decrease observed for Vinton experiments.

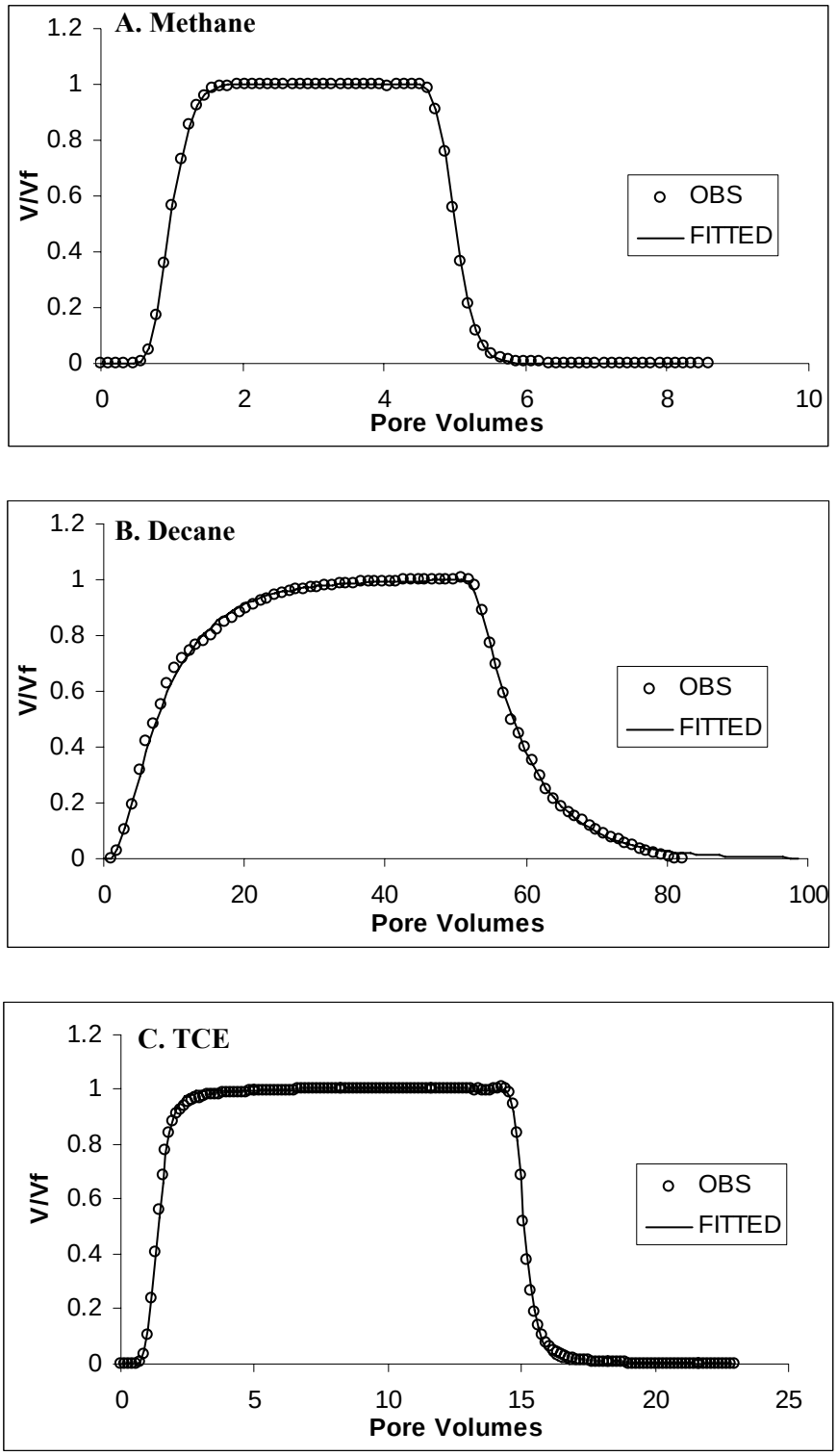


**Figure 3-17.** Representative fitted breakthrough curves using CXTFIT. A) Methane; B) Decane; C) TCE.

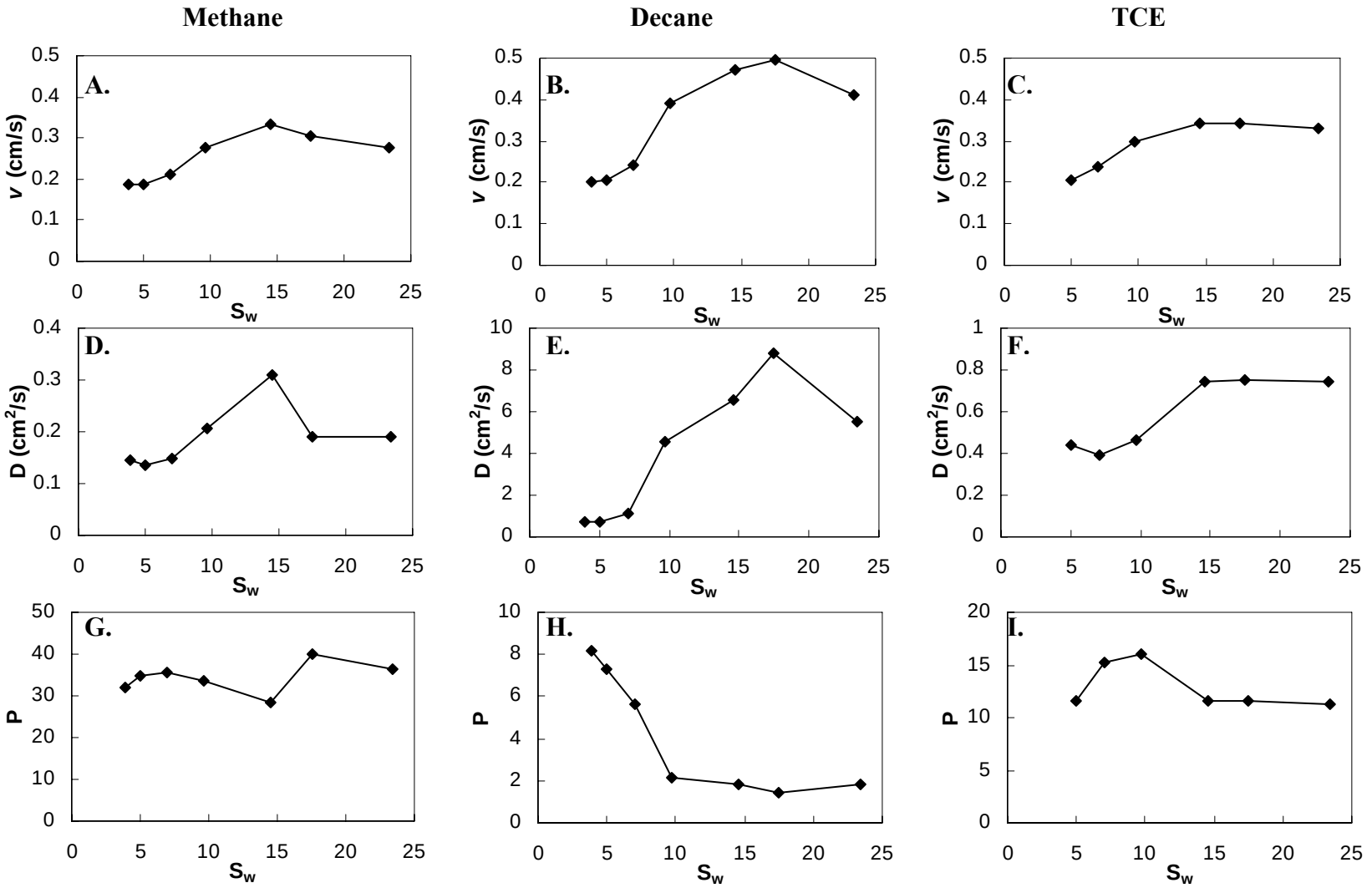


**Figure 3-18.** CXTFIT fitted parameters for Vinton experiments. Raw data, including uncertainties, are listed in the Appendix. A–C) average linear velocity (v); D-F) dispersion coefficient (D); G-I) Peclet number (P).

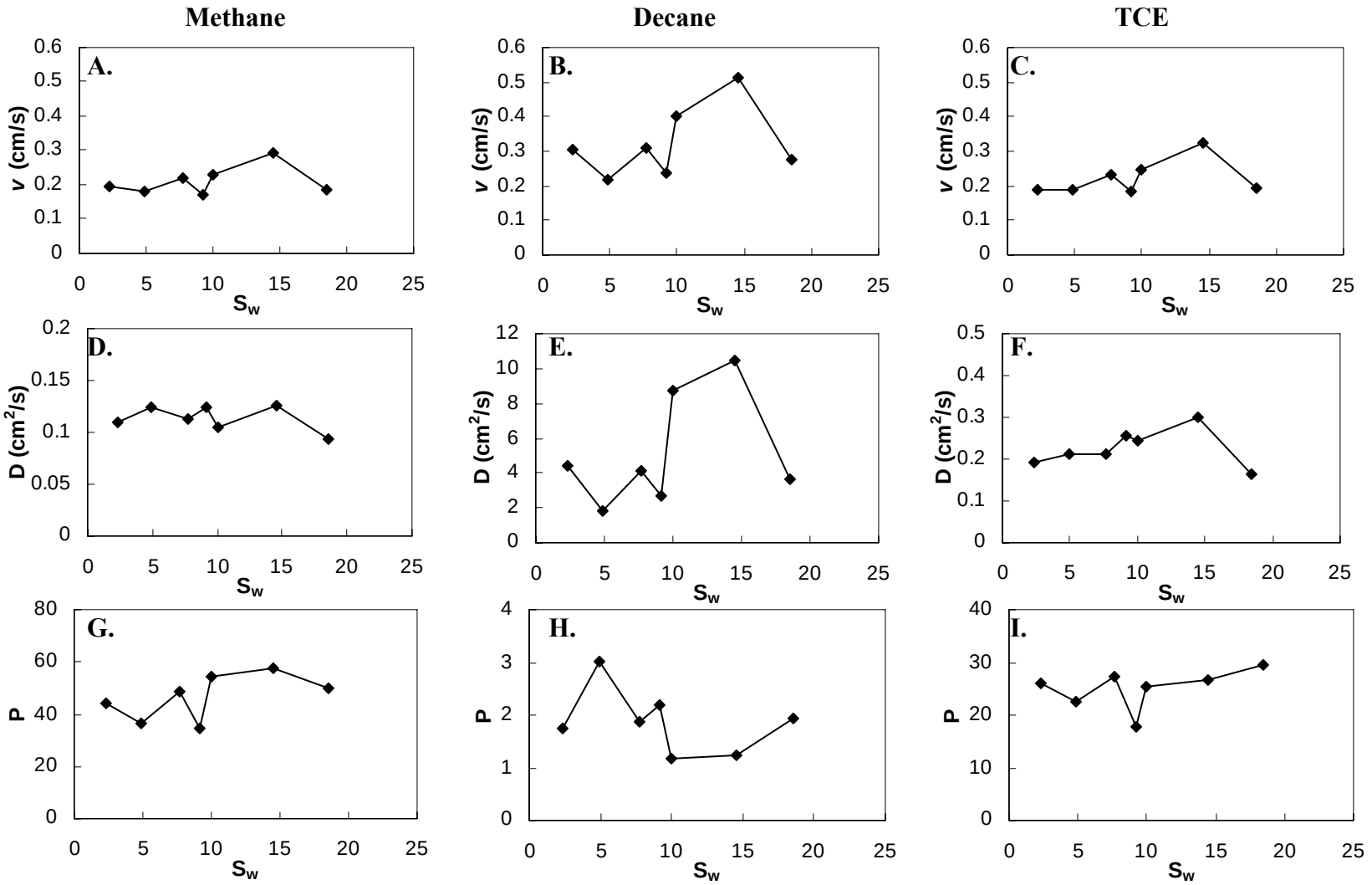


**Figure 3-19.** CXTFIT fitted parameters for Granusil 7030 experiments. Raw data, including uncertainties, are listed in the Appendix. A–C) average linear velocity (v); D-F) dispersion coefficient (D); G-I) Peclet number (P).

# IV. DISCUSSION

*General Air-Water Interfacial Area Trends*

In agreement with previous interfacial tracer studies, $A_{ia}$ continually decreased with increasing $S_w$ over the range studied for both Vinton and Granusil 7030.[10] As shown in Figure 3-14, small variability between replicates indicated high reproducibility of $A_{ia}$ measurements for Vinton. The greater variability at 3.8% $S_w$ may be attributed to some mineral grain adsorption. Because two columns were used to collect data, alternating data points correspond to identical packing for Vinton experiments. Previous studies have shown that similar packing of a media yields similar $A_{ia}$ measurements.[10-11] However, Column B (5.0%, 9.7%, and 17.5% $S_w$) had a slightly greater bulk density, accounting for some of the deviation from a smooth $A_{ia}$-$S_w$ relationship.

As shown in Figure 4-1, the general $A_{ia}$ trend for Vinton was similar to that of the Vinton batch studied by Peng and Brusseau.[11] For all $S_w$, the current work measured $A_{ia}$ to be about 3-5 times larger than those reported by Peng and Brusseau. One explanation for the disparity is the difference in physical properties between the two Vinton media. While most properties were the same, the average bulk density for this study was 1.78 g/cm$^3$, while Peng and Brusseau reported 1.46 g/cm$^3$. For $S_w$ less than 25%, Costanza-Robinson and Brusseau[12] attributed the majority of $A_{ia}$ to the thin-films of adsorbed water surrounding individual grains. A greater bulk density could yield more thin-film interfacial area per unit volume of media, and thus a greater $A_{ia}$.

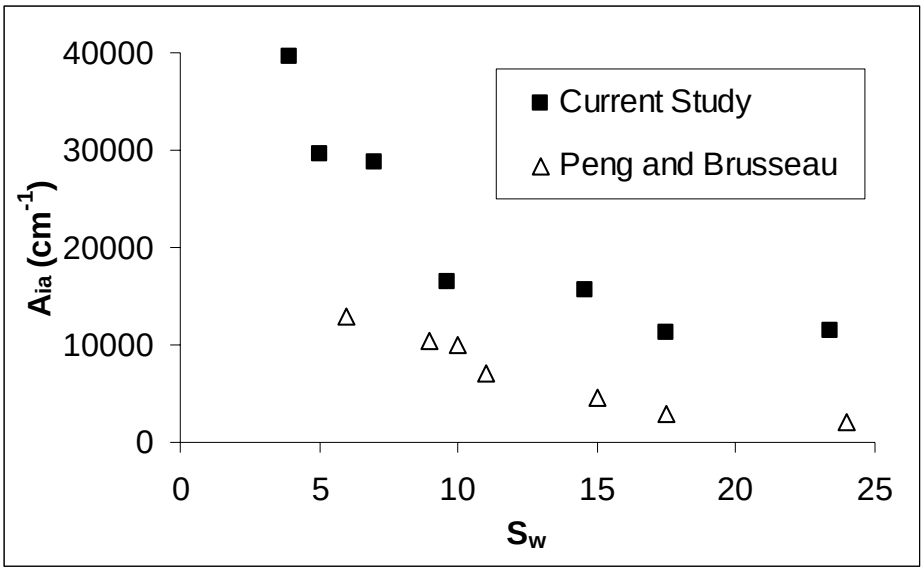


**Figure 4-1.** Averaged measured $A_{ia}$ compared to Peng and Brusseau[11] for Vinton.

In Figure 4-2, the Granusil 7030 $A_{ia}$-$S_w$ relationship is compared to the Granusil 70-100 trend measured by Peng and Brusseau.[11] Although Granusil 70-100 is a slightly finer media than Granusil 7030, it was the most similar data available in the literature. As with Vinton, the measured values in this study were greater than those recorded by Peng and Brusseau, with the disparity increasing at higher $S_w$. Because the bulk density for Granusil 70-100 (1.54 g/cm$^3$) compares favorably with Granusil 7030 (1.50 g/cm$^3$), packing can not explain the observed difference. With other physical properties relatively similar, the explanation for the greater $A_{ia}$ measured in this study may be attributed to uncertainty in the decane interfacial partitioning coefficient.

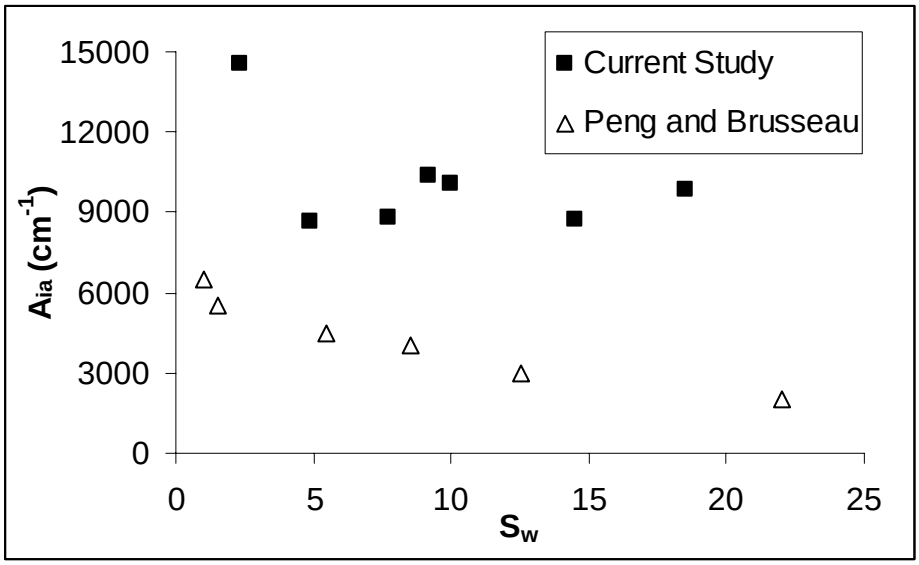


**Figure 4-2.** Averaged measured $A_{ia}$ compared to Peng and Brusseau[11] for Granusil 7030 and Granusil 70-100, respectively.

As with Vinton, replicate experiments had good reproducibility as displayed by the y-error bars in Figure 3-14. The experiments in Column A (4.9% and 9.2% $S_w$) yielded $A_{ia}$ values agreeing with the trend established by Column B. Thus, slightly different packing does not have a significant effect on $A_{ia}$ measurements. The experiment at 18.5% $S_w$ had a value for $A_{ia}$ slightly higher than expected, and will be discussed with fitted Peclet numbers below.

*Normalizing Air-Water Interfacial Areas by Surface-Area*

To compare $A_{ia}$ measurements among studies of different media, $A_{ia}$ is divided by the volume-normalized $N_2$/BET surface area, s, where s = SA × bulk density. Measured $A_{ia}$ values from this study are compared to gas-phase interfacial tracer results from the literature in Figure 4-3. The measured values for Vinton agree reasonably well with the general trend. However, the surface area-normalized $A_{ia}$ for Granusil 7030 is significantly larger than for other studies. Measured $A_{ia}$ values for Granusil 7030 were

actually greater than the $N_2$/BET surface area, and thus, are likely greater than the true values. Nevertheless, except for the data point at 18.5% $S_w$, the general slope agrees with observations for other media. Generally, $A_{ia}$ decreases at a faster rate at lower $S_w$ and gradually levels off. Costanza-Robinson and Brusseau[12] attribute differences among particular studies to varying water-retention properties of the various media. Peng and Brusseau[11] used the slope of the surface area-normalized $A_{ia}$ to give a qualitative description of the particle size distribution. They argue that well-sorted media, such as Granusil, have a smaller rate of $A_{ia}$ change than poorly-sorted media, such as Vinton and the sand studied by Kim et al.[26] Peng and Brusseau[11] argue that this is a result of the sudden change in water morphology for incremental changes in $S_w$ for poorly sorted media.[11]

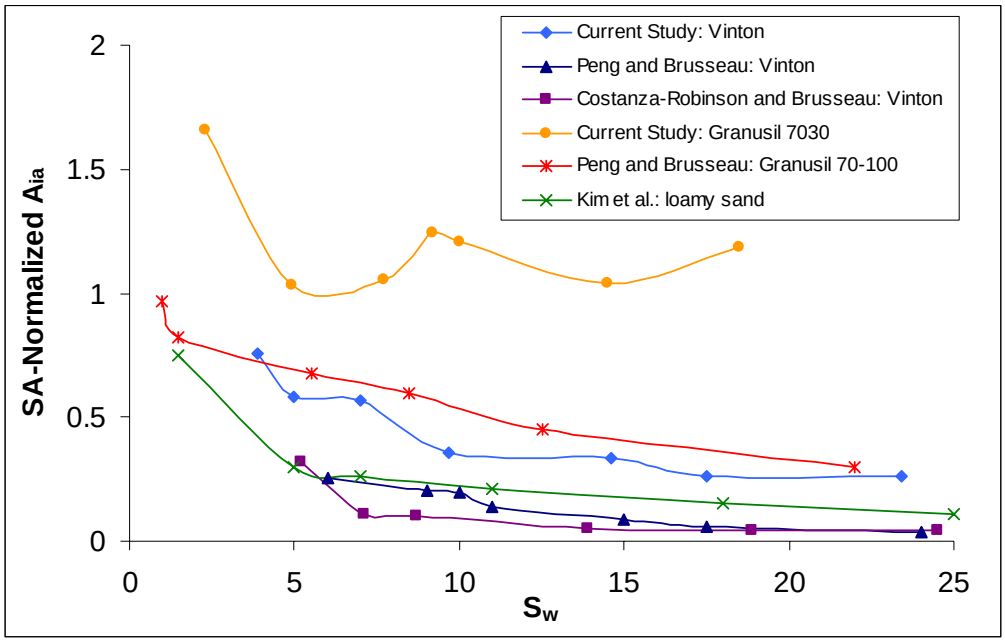


**Figure 4-3.** Surface-area normalized $A_{ia}$-$S_w$ relationship with comparison to gas-phase tracer results in literature.[11-12, 26] Measurements are normalized by $N_2$/BET surface areas.

*Normalizing Air-Water Interfacial Areas by Monolayer Saturation*

Theoretically, at very low $S_w$, $A_{ia}$ must drop to zero as complete water coverage of the media is no longer maintained. However, at such low $S_w$, mineral grain adsorption becomes the dominant retention process, and the gas-phase tracer technique for measuring $A_{ia}$ is not applicable. As presented in Chapter II, the degree to which mineral grains are exposed can be quantified by the number of effective water monolayers present, and is represented by $S_w/S_m$. Surface area-normalized $A_{ia}$ is shown for Vinton as a function of the number of effective monolayers and compared to Peng and Brusseau[11] in Figure 4-4. Normalizing $A_{ia}$ by surface area and $S_w$ by $S_m$ yields the best agreement between the two studies, as expected. Peng and Brusseau considered Vinton experiments below 6 monolayers to have been influenced by soil vapor adsorption, and thus, have artificially high values for measured $A_{ia}$. At 3.8% $S_w$ for Vinton in this study, the number of effective monolayers is 7.5, most likely on the borderline of acceptability. Because the measured $A_{ia}$ at 3.8% $S_w$ was still below the $N_2$/BET surface area, and therefore reasonable, it was included in all analyses.

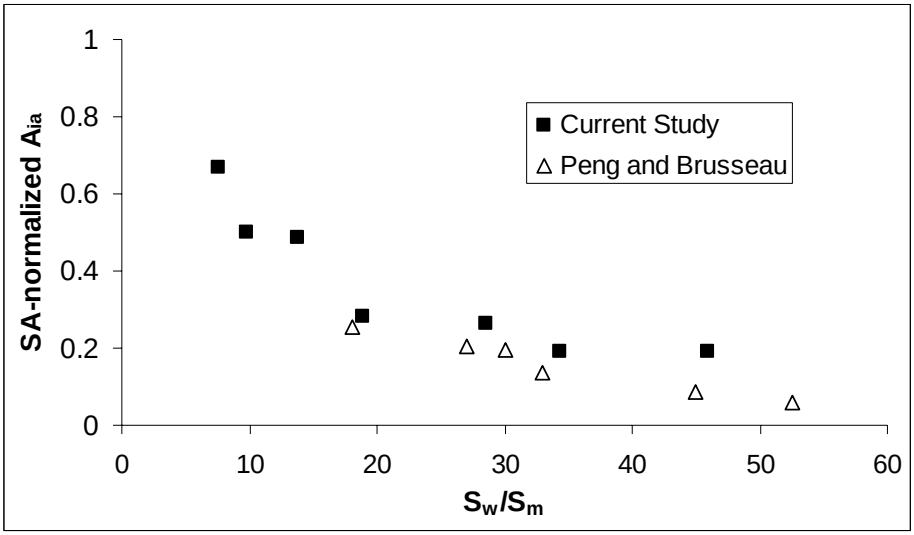


**Figure 4-4.** Surface area-normalized $A_{ia}$-$S_w/S_m$ relationship for Vinton in this study compared to Peng and Brusseau.[11]

Granusil 7030, with a smaller surface area, has more effective monolayers for a given $S_w$ than Vinton. At 2.3% $S_w$, there were still 41.8 effective monolayers, and therefore retention was most likely not affected by mineral grain adsorption. However, as mention above, measured $A_{ia}$ still exceeded the $N_2$/BET surface area. Surface area- and $S_m$-normalized $A_{ia}$ measurements are compared to Peng and Brusseau[11] in Figure 4-5. Although the results agree slightly better than the non-normalized values in Figure 4-2, $A_{ia}$ values measured here are still significantly greater than equivalent literature values.

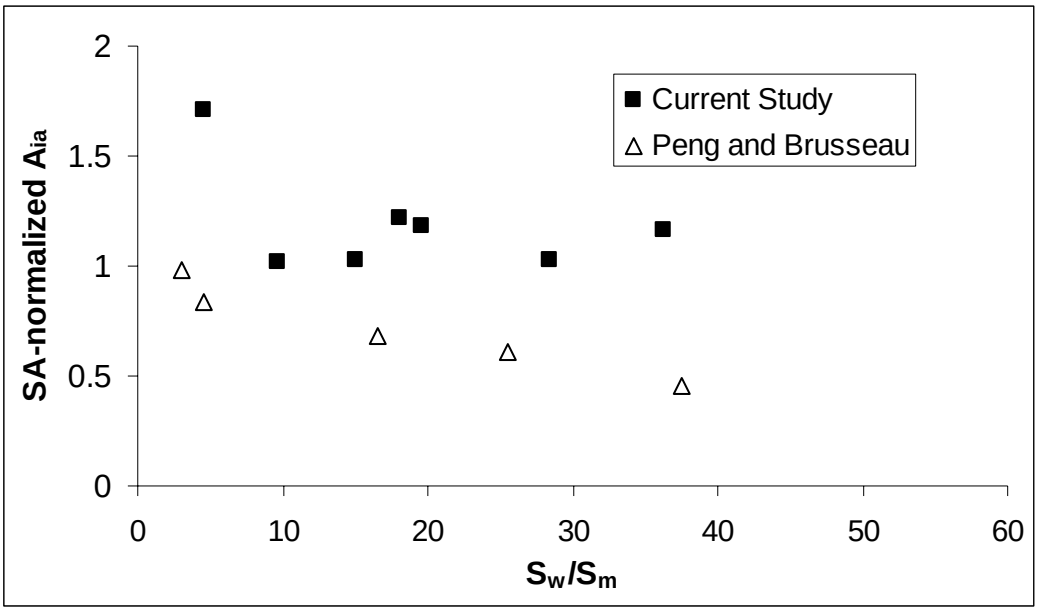


**Figure 4-5.** Surface-area normalized $A_{ia}$-$S_w/S_m$ relationship for Granusil 7030 in this study compared to Peng and Brusseau.[11]

*Predicting Air-Water Interfacial Area Trends*

In 1980, Van Genuchten expressed a functional relationship between $S_w$ and capillary pressure.[41] Peng and Brusseau[11] modified the equation to describe the behavior of $A_{ia}$ based on $S_w$ as

$$A_{ia} = s[1 + (\alpha(S_w - S_m))^n]^{-m} \qquad [4\text{-}1]$$

where

$$n = \frac{1}{2 - m} \qquad [4\text{-}2]$$

α and m are fitted parameters (-), s is the volume-normalized $N_2$/BET surface area ($s = SA \times \rho_b$), $S_w$ (-) and $S_m$ (-) have been defined previously. Using data from six porous media, Peng and Brusseau[11] fit relationships for α and m as functions of the uniformity coefficient, U. These are given as

$$\alpha = 14.3 \ln(U) + 3.72 \qquad [4\text{-}3]$$

$$m = \begin{cases} -0.098U + 1.53, & U < 3.5 \\ 1.2, & U \geq 3.5 \end{cases} \qquad [4\text{-}4]$$

Using Equations 4-3 and 4-4, α and m were estimated at 16.24 and 1.29, respectively for Vinton. For Granusil 7030, α and m were estimated at 11.31 and 1.36. These parameters were used to predict the relationship between $A_{ia}$ and $S_w$, and are compared to the measured $A_{ia}$ values in Figure 4-6. Overall, the predictions agreed more closely with measured values for Vinton than Granusil 7030. Generally, predicted $A_{ia}$ had better agreement with measured values at lower $S_w$. Discrepancy between predicted and measured values is most likely due to error in estimates for α and m, and uncertainty in measured $A_{ia}$ values. Therefore, Equation 4-1 was optimized for these fitting parameters by allowing α and m to vary by up to 100% until minimal error between predicted and measured $A_{ia}$ was achieved. The averaged optimized parameters were averaged over all Vinton experiments yielding values of 16.23 and 1.21 for α and m, respectively. For Granusil 7030 experiments, optimization produced negative numbers, which is an indication that the fitting boundaries were not sufficient. The measured $A_{ia}$ for Granusil 7030 in this study was significantly higher than expected (e.g. larger than the

$N_2$/BET surface area), and could not be modeled using Equation 4-1. The optimized predictions for Vinton are shown in Figure 4-7. The improved fit indicates that $A_{ia}$ may be predicted to a certain degree once physical bases for α and m parameters are better understood.

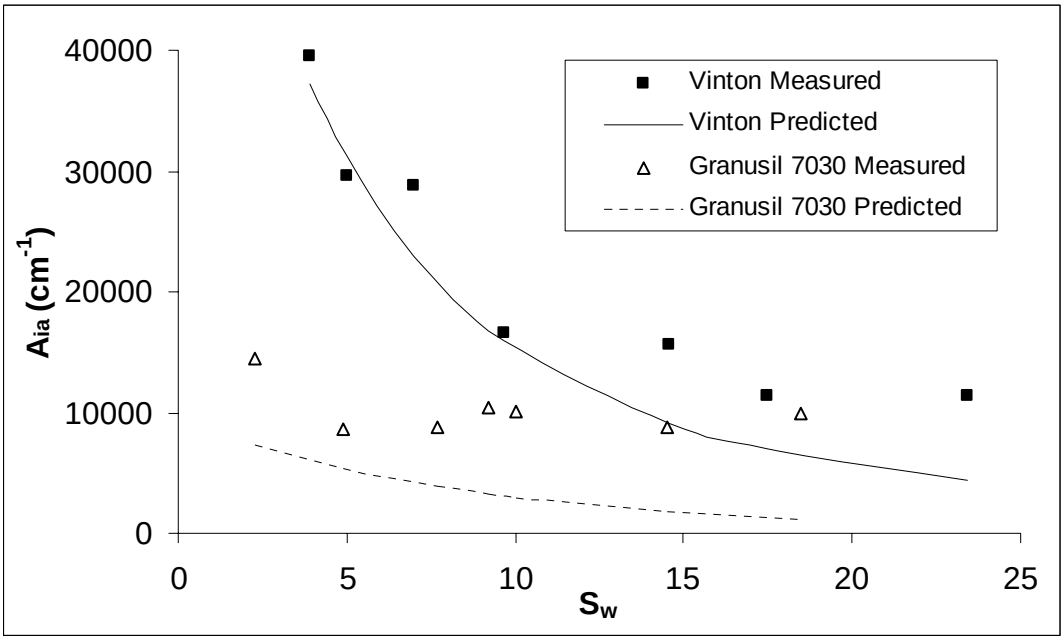


**Figure 4-6.** Predicted $A_{ia}$-$S_w$ relationship using Equation 4-1.

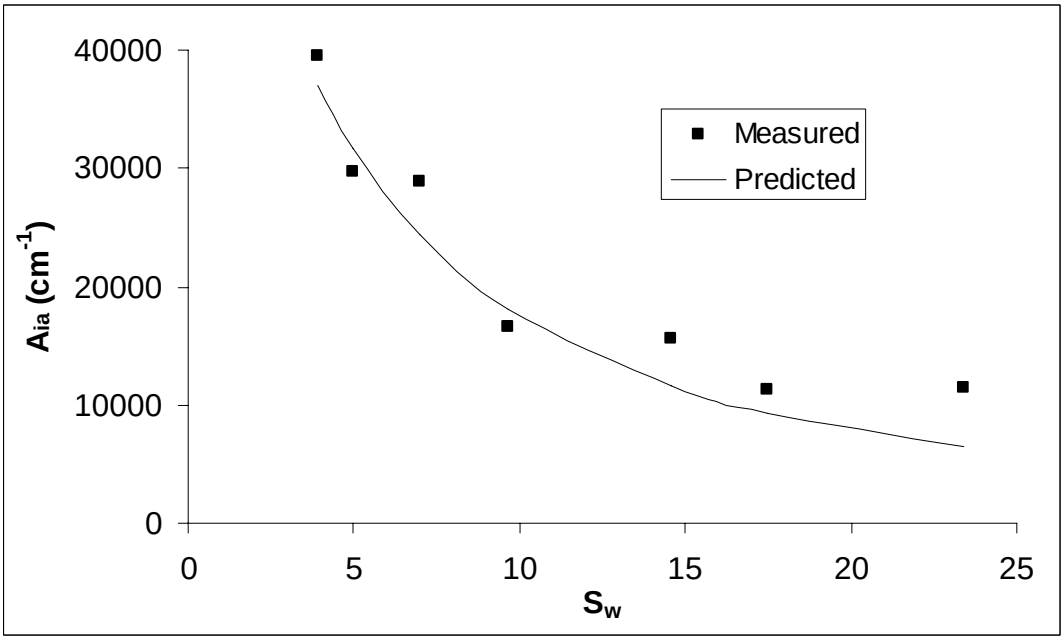


**Figure 4-7.** Optimized prediction of $A_{ia}$-$S_w$ relationship for Vinton using Equation 4-1.

*CXTFIT: Dispersion and Peclet Numbers*

Modeling breakthrough curves with CXTFIT allowed for a quantitative measure of the degree of dispersion and a subsequent calculation of the Peclet number as shown in Figures 3-18 and 3-19. Larger Peclet numbers signify more ideal flow, with less dispersion. The total dispersion is a sum of the diffusive and the mechanical mixing components, and is given by the equation:

$$D = D_a \tau + \alpha \nu \qquad [4\text{-}5]$$

where $D_a$ is the binary molecular diffusion coefficient in air ($cm^2/s$), $\tau$ is the tortuosity factor, inversely proportional to tortuosity (-), $\alpha$ is the gas-phase longitudinal dispersivity (cm), and $\nu$ is the average linear velocity (cm/s). Because the volumetric flux was kept constant, experiments at higher $S_w$ had greater average linear velocities. The flux at 18.5% $S_w$ for Granusil 7030 was most likely low, and thus, this data point was a notable outlier for all trends in Figure 3-19. Although the diffusion term is independent of velocity, the mechanical mixing component increases with increasing $\nu$. Thus, the total dispersion coefficient generally increased with $S_w$. Methane, which has the greatest diffusion, remained relatively constant because it has a smaller percent of the total dispersion attributed to mechanical mixing. Similarly, the Peclet numbers for decane and TCE experiments generally decreased with increasing $S_w$ as a result of increased dispersion coefficients.

Costanza-Robinson[4] found methane dispersion to generally decrease with increasing $S_w$, while Peclet numbers tended to increase. However, because that study used lower linear velocities, smaller Peclet numbers were attained. Garges and Baehr[42] found that for Peclet numbers greater than 10, mechanical mixing tends to dominate the

system. Costanza-Robinson[4] reported Peclet numbers less than 10, and thus, more of the dispersion was attributed to diffusion. Experiments at higher $S_w$ have shorter residence time, and consequently less total diffusion. For this study, mechanical mixing was likely a larger factor, and thus total dispersion remained constant.

*Predicting TCE Retardation*

One of the primary reasons to measure $A_{ia}$ is to be able to predict the transport of contaminants through the vadose zone. After calculating the $A_{ia}$ for Vinton and Granusil 7030, the retardation of TCE was predicted using Equation 2-1 and published values for $K_h$, $K_D$, and $K_{ia}$. The predicted retardation factors for both media reflected the general trend of the measured values closely (Figures 3-15 and 3-16). For both media, TCE retardation decreased to a minimum and then increased with $S_w$. This is due to the greater aqueous solubility of TCE, and corresponding dissolution into the bulk water. For all $S_w$, however, the predicted retardation factors were larger than the observed values. One explanation is uncertainties in $K_{ia}$ because of the few values reported in the literature, and the difficulty measuring it.[4]

To assess the effect of varying $K_{ia}$, TCE retardation factor predictions were optimized based on the measured values by simultaneously solving Equation 2-1 for decane and TCE $K_{ia}$. This could then be rewritten as a ratio of the two adsorption coefficients:

$$\frac{K_{ia,Dec}}{K_{ia,TCE}} = \frac{R^{Dec} - 1 - \dfrac{\rho_b K_{d,Dec}}{\theta_a K_{h,Dec}} - \dfrac{\theta_w}{\theta_a K_{h,Dec}}}{R^{TCE} - 1 - \dfrac{\rho_b K_{d,TCE}}{\theta_a K_{h,TCE}} - \dfrac{\theta_w}{\theta_a K_{H,TCE}}} \qquad [4\text{-}6]$$

The measured ratio is plotted at each $S_w$ for Vinton and Granusil 7030 in Figures 4-8 and 4-9, respectively. The initial ratio: $\frac{K_{ia,Dec}}{K_{ia,TCE}} = \frac{2.2\times10^{-4}\,cm}{2.64\times10^{-5}\,cm} = 8.48$ is smaller than all observed data. Excluding the outlier at 23.4% $S_w$, Vinton experimental ratios ranged from 29 to 70, with an average of 38. Granusil 7030 experimental ratios ranged from 9 to 54, with an average of 30.

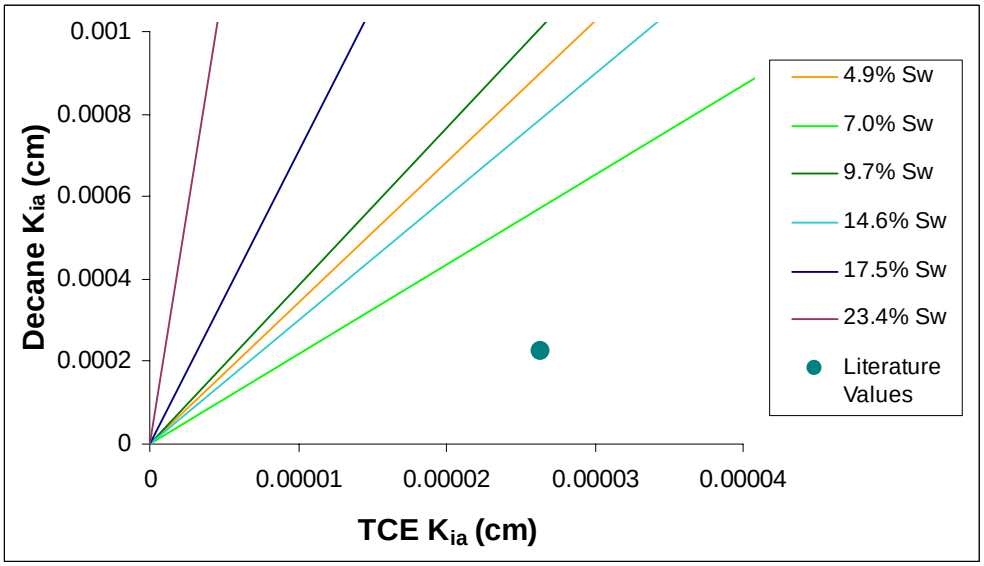


**Figure 4-8**. Optimized decane:TCE $K_{ia}$ ratios for Vinton experiments.

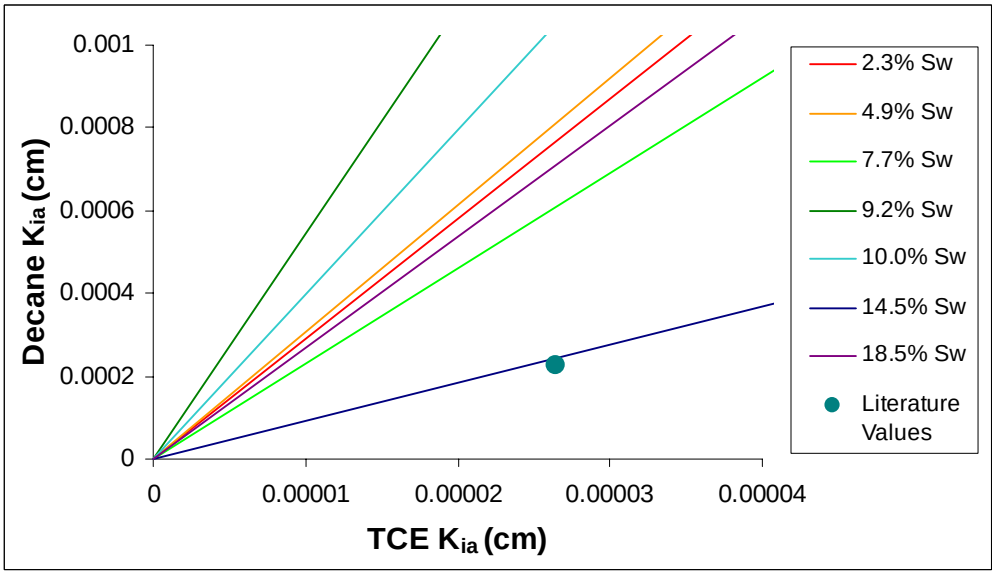


**Figure 4-9**. Optimized decane:TCE $K_{ia}$ ratios for Granusil 7030 experiments.

For both media, the optimized $K_{ia}$ ratio of decane to TCE was greater than the ratio of values obtained from the literature. At 25 °C, the TCE $K_{ia}$ value of $2.64 \times 10^{-5}$ cm reported by Hoff et al.[8] agrees with a later measurement of $2.70 \times 10^{-5}$ cm by Bruant and Conklin.[43] For decane, Karger et al.[44] originally reported $K_{ia}$ as $5.3 \times 10^{-4}$ cm at 12.5 °C. Hoff et al.[8] measured decane $K_{ia}$ as $2.24 \times 10^{-4}$ cm at 25 °C, while Roth et al.[45] reported a value of $4.68 \times 10^{-4}$ cm at 15 °C. Lei et al.[46] recently found $K_{ia}$ to fluctuate significantly with temperature for $C_4 - C_{10}$ alkanols. The temperature of the gases in the column is less than 25 °C, due to ambient temperatures in the laboratory (~21 °C), gas expansion upon leaving the high pressure cylinders, and contact with the stainless steel apparatus. At lower system temperatures, fewer molecules will enter the gas phase, leading to larger values for $K_{ia}$.

TCE predicted retardation factors were calculated using the optimized decane to TCE $K_{ia}$ ratio of 34, as shown in Figure 4-10. Assuming TCE $K_{ia}$ remains fixed at $2.64 \times 10^{-4}$ cm, this optimized ratio would correspond to decane $K_{ia}$ of $9 \times 10^{-4}$ cm. Using this value for decane $K_{ia}$ would significantly lower $A_{ia}$ estimations for both media. In fact, a decane $K_{ia}$ greater than $3.7 \times 10^{-4}$ cm (65% increase) would reduce Granusil 7030 $A_{ia}$ estimations below the $N_2$/BET surface area. Using a similar optimization method, Costanza-Robinson reported a ratio-derived value decane $K_{ia}$ of $6.2 \times 10^{-4}$ cm. The optimized partitioning coefficient can be related to a specific temperature assuming linear $\ln(K_{ia})$-1/T relationship of the literature data.[46] As shown in Figure 4-11, using a linear regression, a decane $K_{ia}$ of $9 \times 10^{-4}$ cm would corresponded to a gas temperature of 5 °C. Although this is most likely a temperature underestimation, and consequently overestimation of decane $K_{ia}$, it is still reasonably possible. To predict the retardation of

TCE, the exact partitioning coefficients are not as important as the ratio between the two. Optimizing this ratio greatly improves the agreement between measured and predicted TCE retardation factors for both media.

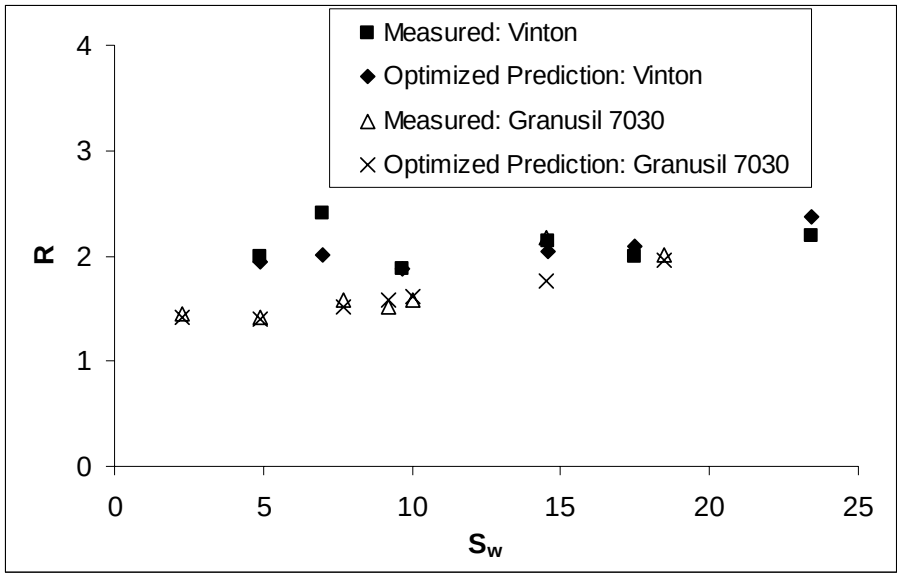


**Figure 4-10**. Optimized predictions for the retardation of TCE. A value of $9 \times 10^{-4}$ cm was used for decane $K_{ia}$.

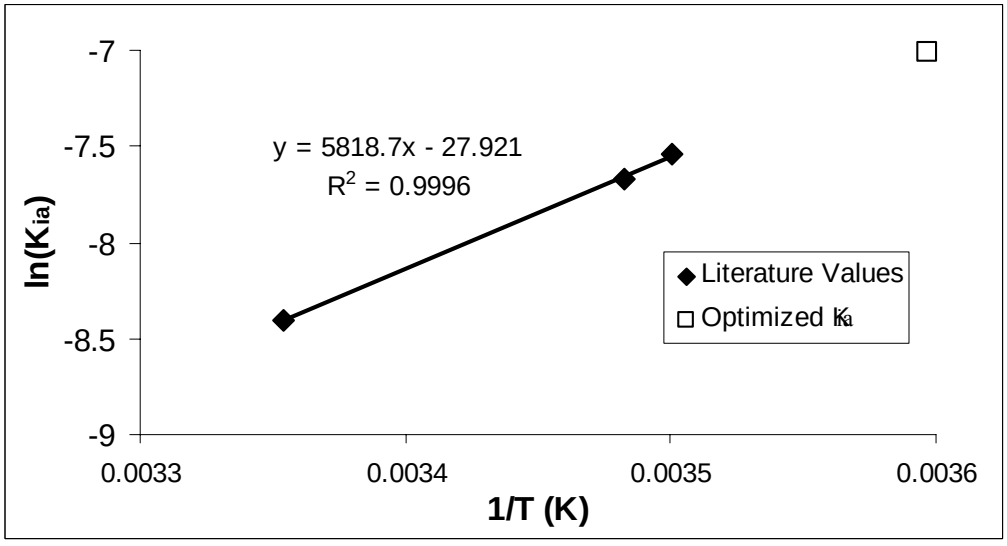


**Figure 4-11**. The $\ln(K_{ia})$-1/T relationship of literature decane data.[8,44-45] Optimized $K_{ia}$ corresponds to a temperature of 5 °C.

# V. CONCLUSION AND FUTURE WORK

Air-water interfacial areas ($A_{ia}$) were measured at seven water saturations ($S_w$) for both Vinton and Granusil 7030 using a gas-phase interfacial tracer. At all $S_w$, the Vinton media exhibited higher $A_{ia}$ than Granusil 7030. This agrees with the hypothesis that surface roughness is a principle variable controlling water morphology, and thus size of the air-water interface. Both Granusil 7030 and Vinton had similar areas under the smooth sphere approximation. However, the surface roughness of Vinton yields a much larger $N_2$/BET area, and consequently greater retardation of contaminant transport. Thus, the gas-phase interfacial tracer technique can detect surface roughness associated with a particular porous medium.

Using the measured $A_{ia}$ values, TCE retardation factors were predicted and compared to observed values. For both media, the predicted TCE retardation followed the same general pattern as the measured values. However, for all $S_w$, the predicted retardation was greater than what was observed. One possible explanation for the increased predicted retention is the uncertainty in the $K_{ia}$ for decane.[4] $K_{ia}$ varies with temperature, with lower temperatures corresponding to increased adsorption at the air-water interface. Thus, column temperatures lower than 25 °C would lead to increased interfacial sorption and predictions more consistent with the measured values.

There are still several questions from this study yet to be answered. First of all, it is unknown why measured stainless steel sorption was significantly larger than reported by Costanza-Robinson.[4] It is possible that temperature differences may explain this disparity, and a temperature study should be included in the next step of the project. This may also clarify whether interfacial tracers can be used effectively to predict TCE

retardation. In the environment, it would be beneficial to understand how contaminants behave in different climates or seasons.

Secondly, wetting methods for achieving low $S_w$ need to be improved. It is difficult to assess whether the baking method, described by Kim et al.[26] and used in this study, is representative of natural conditions. Standard imbibition and drainage cycles do not reach the lowest $S_w$, where thin-films have the greatest importance.

Once the measurements for this study have been validated, the next step is to include other porous media and a variety of contaminants. Ideally, the decane-derived $A_{ia}$ values should be applicable for any contaminant known to sorb at the air-water interface. Finally, the gas-phase interfacial tracer derived $A_{ia}$ will be compared to values measured using computer-assisted X-ray microtomography. The current hypothesis is that the two techniques are measuring different interfaces. Using the ratio between the $N_2$/BET area and the smooth-sphere approximated areas, a proxy for surface roughness, ideally the two different measurements for $A_{ia}$ may be compared. This comparison would allow identification of the interfacial domains being measured by each technique.

# LITERATURE CITED


1. Zogorski, J.S.; Carter, J.M.; Ivahnenko, T.; Lapham, W.W., Moran, M.J.; Rowe, B.L.; Squillace, P.J.; Toccalino, P.L. The quality of our Nation's waters—Volatile organic compounds in the Nation's ground water and drinking-water supply wells. U.S. Geological Survey Circular 1292, 2006.
2. "Soil Vapor Extraction." Hazardous Waste Clean-Up Information web site for the United States Environmental Protection Agency. Visited on 30 April 2007 <http://clu-in.org>.
3. "In Situ Physical/Chemical Treatment: Soil Vapor Extraction." Federal Remediation Technologies Roundtable: Remediation Technologies Screening Matrix and Reference Guide. Visited on 30 April 2007 <http://www.frtr.gov/matrix2/section4/4-7.html>.
4. Costanza-Robinson, M.S. The elucidation of retention processes governing the transport of volatile organic compounds in unsaturated soil systems. Ph.D. Dissertation, The University Of Arizona, Tucson, AZ, 2001, 118.
5. Brusseau, M. L.; Popovicova, J.; Silva, J. A. K. Characterizing gas-water interfacial and bulk-water partitioning for gas-phase transport of organic contaminants in unsaturated porous media. *Environ. Sci. Technol*. **1997,** *31,* 1645-1649.
6. Lorden, S. W.; Chen, W.; Lion, L. W. Experiments and modeling of the transport of trichloroethene vapor in unsaturated aquifer material. *Environ. Sci. Technol*. **1998,** *32,* 2009-2017.
7. Pennel, K. D.; Rhue, R. D.; Rao, P. S.; Johnston, C. T. Vapor-phase sorption of p-xylene and water on soils and clay minerals. *Environ. Sci. Technol*. **1992,** *26,* 756-763.
8. Hoff, J. T.; Mackay, D.; Gillham, R.; Shlu, W. Y. Partitioning of organic chemicals at the air-water interface in environmental systems. *Environ. Sci. Technol*. **1993,** *27,* 2174-2180.
9. Hoff, J. T.; Mackay, D.; Gillham, R.; Shlu, W. Y. Sorption of organic vapors at the air-water interface in a sandy aquifer material. *Environ. Sci. Technol*. **1993,** *27,* 2789-2794.
10. Costanza, M.S.; Brusseau, M.L. Contaminant vapor adsorption at the gas-water interface in soils. *Environ. Sci. Technol.* **2000,** *34,* 1-11.
11. Peng, S.; Brusseau, M.L. Impact of soil texture on air-water interfacial areas in unsaturated sandy porous media. *Water Resour. Res.* **2005,** *41,* W03021.
12. Costanza-Robinson, M.S.; Brusseau, M.L. Air-water interfacial areas in unsaturated soils: Evaluation of interfacial domains. *Water Resour. Res.* **2002,** *38,* 1195.
13. Wan, J.; Wilson, J. L. Visualization of the role of the gas-water interface on the fate and transport of colloids in porous media. *Water Resour. Res.* **1994,** *30,* 11-23.
14. Wan, K.; Tokunaga, T. K. Measuring partition coefficients of colloids at air-water interfaces. *Environ. Sci. Technol.* **1998,** *32,* 3293-3298.
15. Schäfer, A.; Harms, H.; Zehnder, A. J. B. Bacterial accumulation at the air-water interface. *Environ. Sci. Technol.* **1998,** *32,* 3704-3712.
16. Donaldson, D. J.; Anderson, D. Adsorption of atmospheric gases at the air-water interface. *J. Phys. Chem. A.* **1999,** *103,* 871-876.

17. Bryant, S.; Johnson, A. Bulk and film contributions to fluid/fluid interfacial area in granular media. *Chem. Eng. Comm.* **2004,** *191,* 1660-1670.
18. Gvirtzman, H.; Roberts, P. V. Pore scale spatial analysis of two immiscible fluids in porous media. *Water Resour. Res.* **1991,** *27,* 1165-1176.
19. Reeves, P. C.; Celia, M. A. A functional relationship between capillary pressure, saturation, and interfacial area as revealed by a pore-scale network model. *Water Resour. Res.* **1996,** *32,* 2345-2358.
20. Cary, J. W. Estimating the surface area of fluid phase interfaces in porous media. *J. Contam. Hydrol*. **1994,** *15,* 243-248.
21. Or, D.; Tuller, M. Liquid retention and interfacial area in variably saturated porous media: upscaling from single-pore to sample-scale model. *Water Resour. Res.* **1999,** *35,* 3591-3605.
22. Silverstein, D. L.; Fort, T. Prediction of air-water interfacial area in wet unsaturated porous media. *Langmuir.* **2000,** *16,* 829-834.
23. Brusseau, M.L.; Nelson, N.T.; Costanza-Robinson, M.S. Partitioning tracer tests for characterizing immiscible-fluid saturations and interfacial areas in the vadose zone. *Vadose Zone J.* **2003,** *2*, 138-147.
24. Saripalli, K. P.; Kim, H.; Rao, P. S. C.; Annable, M. D. Measurement of specific fluid-fluid interfacial areas of immiscible fluids in porous media. *Environ. Sci. Technol.* **1997,** *31,* 932-936.
25. Kim, H.; Rao, P. S. C. Determination of effective air-water interfacial area in partially saturated porous media using surfactant adsorption. *Water Resour. Res.* **1996,** *33,* 2705-2711.
26. Kim, H.; Rao, P. S. C. Gaseous tracer technique for estimating air-water interfacial areas and interface mobility. *Soil Sci. Soc. Am. J.* **1999,** *63,* 1554-1560.
27. Kim, H.; Rao, P. S. C. Determination of effective air-water interfacial area in partially saturated porous media using surfactant adsorption. *Water Resour. Res.* **1997,** *35,* 2705-2711.
28. Kim, H.; Annable, M. D.; Rao, P. S. C. Influence of air-water interfacial adsorption and gas-phase partitioning on the transport of organic chemicals in unsaturated porous media. *Environ. Sci. Technol*. **1998,** *32,* 1253-1259.
29. Karkare, M. V.; Hoa, T. L.; Fort, T. Criteria for effectiveness of surfactants as water-moving agents in "unsaturated" wet sand. *Langmuir.* **1993,** *9,* 1684-1690.
30. Anwar, A. H. M. F.; Bettahar, M.; Matsubayashi, U. A method for determining air-water interfacial area in variably saturated porous media. *J. Contam. Hydrol*. **2000,** *43,* 129-146.
31. Schaefer, C. E.; DiCarlo, D. A.; Blunt, M. J. Experimental measurement of air-water interfacial area during gravity drainage and secondary imbibition in porous media. *Water Resour. Res.* **2000,** *36,* 885-890.
32. Wildenschild, D.; Hopmans, J. W.; Vaz, C. M. P.; Rivers, M. L.; Rolard, D. Christensen, B. S. B. Using X-ray computed tomography in hydrology: systems, resolutions, and limitations. *J. Hydrol*. **2002,** *267,* 285-297.
33. Culligan, K.A.; Wildenschild, D.; Christensen, B.S.B.; Gray, W.G.; Rivers, M.L.; Tompson, A.F.B. Interfacial area measurements for unsaturated flow through a porous medium. *Water Resour. Res.* **2004,** *40,* W12413.

34. Wildenschild, D.; Hopmans, J. W.; Rivers, M. L.; Kent, A. J. R. Quantitative analysis of flow processes in a sand using synchrotron-based X-ray microtomography. *Vadose Zone J*. **2005,** *4,* 112-126.
35. Schnaar, G.; Brusseau, M. L. Pore-scale characterization of organic immiscible-liquid morphology in natural porous media using synchrotron X-ray microtomography. *Environ. Sci. Technol*. **2005,** *39,* 8403-8410.
36. Brusseau, M. L.; Peng, S.; Schnaar, G.; Murao, A. Measuring air–water interfacial areas with x-ray microtomography and interfacial partitioning tracer tests. *Environ. Sci. Technol*. **2007,** *41,* 1956-1961.
37. Ketcham, R.A.; Carlson, W.D. Acquisition, optimization and interpretation of X-ray computed tomographic imagery: applications to the geosciences. *Computers & Geosciences* **2001,** *27,* 381-400.
38. Lyman, W. J. 1990. "Adsorption Coefficient for Soils and Sediments." *Handbook of Chemical Property Estimation Methods: Environmental Behavior of Organic Compounds*. W. J. Lyman, editor. American Chemical Society, Washington DC.
39. Schwarzenbach, R. P.; Gschwend, P. M.; Imboden, D. M. 2003. *Environmental Organic Chemistry*. John Wiley and Sons, Inc., New Jersey.
40. Leij, N. T.; van Genuchten, M. Th. The CXTFIT code for estimating transport parameters from laboratory or field tracer experiments. Version 2.1. Agricultural Research Service, U. S. Department of Agriculture, **1999**.
41. van Genuchten, M. T. A closed-form equation for predicting the hydraulic conductivity of unsaturated soils. *Soil Sci. Soc. Am. J.* **1980,** 44, 892-898.
42. Garges, J. A.; Baehr, A. L. Type curves to determine the relative importance of advection and dispersion for solute and vapor transport. *Ground Water* **1998,** 36, 959-965.
43. Bruant, R. J.; Conklin, M. H. Adsorption of trichloroethene at the vapor/water interface. *Environ. Sci. Technol*. **2001,** 35, 362-364.
44. Karger, B. L; Castells, R. C.; Sewell, P. A.; Hartkopf, A. Study of the adsorption of insoluble and sparingly soluble vapors at the gas-liquid interface of water by gas chromatography. *J. Phys. Chem.* **1971,** 75, 3870-3879.
45. Roth, C. M.; Goss, K.; Schwarzenbach, R. P. Adsorption of a diverse set of organic vapors on the bulk water surface. *J. Colloid Interface Sci.* **2002,** 252, 21-30.
46. Lei, Y. D.; Shunthirasingham, C.; Wania, F. Comparison of headspace and gas-stripping techniques for measuring the air-water partitioning of normal alkanols (C4 to C10): Effect of temperature, chain length, and adsorption to the water surface. *J. Chem. Eng. Data* **2007,** 52, 168-179.

# APPENDIX

**Table A-1. CXTFIT Fitted Parameters for Vinton Experiments**

| | Methane | | | Decane | | | TCE | | |
|---|---|---|---|---|---|---|---|---|---|
| $S_w$ (%) | υ (cm/s) | D ($cm^2/s$) | P (-) | υ (cm/s) | D ($cm^2/s$) | P (-) | υ (cm/s) | D ($cm^2/s$) | P (-) |
| 3.9 | 0.186 ± 0.002 | 0.146 ± 0.009 | 31.9 ± 2.3 | 0.201 ± 0.001 | 0.732 ± 0.213 | 8.2 ± 0.5 | NA | NA | NA |
| 5.0 | 0.189 ± 0.003 | 0.134 ± 0.008 | 35.0 ± 1.4 | 0.205 ± 0.003 | 0.731 ± 0.023 | 7.3 ± 0.3 | 0.204 ± 0.005 | 0.441 ± 0.047 | 11.6 ± 0.9 |
| 7.0 | 0.211 ± 0.003 | 0.148 ± 0.006 | 35.8 ± 1.1 | 0.244 ± 0.004 | 1.092 ± 0.120 | 5.6 ± 0.5 | 0.240 ± 0.005 | 0.392 ± 0.025 | 15.3 ± 0.7 |
| 9.7 | 0.278 ± 0.002 | 0.206 ± 0.001 | 33.7 ± 0.3 | 0.393 ± 0.012 | 4.590 ± 0.902 | 2.2 ± 0.3 | 0.299 ± 0.006 | 0.465 ± 0.017 | 16.1 ± 0.3 |
| 14.6 | 0.335 ± 0.008 | 0.308 ± 0.094 | 28.5 ± 6.9 | 0.472 ± 0.001 | 6.540 ± 0.280 | 1.8 ± 0.1 | 0.342 ± 0.006 | 0.742 ± 0.051 | 11.5 ± 0.6 |
| 17.5 | 0.305 ± 0.002 | 0.191 ± 0.004 | 40.0 ± 0.7 | 0.498 ± 0.010 | 8.768 ± 0.749 | 1.4 ± 0.1 | 0.344 ± 0.004 | 0.752 ± 0.085 | 11.5 ± 1.1 |
| 23.4 | 0.276 ± 0.004 | 0.189 ± 0.008 | 36.5 ± 1.0 | 0.412 ± 0.002 | 5.549 ± 0.320 | 1.9 ± 0.1 | 0.333 ± 0.009 | 0.744 ± 0.093 | 11.3 ± 1.1 |

**Table A-2. CXTFIT Fitted Parameters for Granusil 7030 Experiments**

| | Methane | | | Decane | | | TCE | | |
|---|---|---|---|---|---|---|---|---|---|
| $S_w$ (%) | υ (cm/s) | D ($cm^2/s$) | P (-) | υ (cm/s) | D ($cm^2/s$) | P (-) | υ (cm/s) | D ($cm^2/s$) | P (-) |
| 2.3 | 0.194 ± 0.001 | 0.110 ± 0.003 | 44.2 ± 1.0 | 0.303 ± 0.019 | 4.403 ± 0.687 | 1.7 ± 0.2 | 0.189 ± 0.046 | 0.192 ± 0.082 | 26.0 ± 5.2 |
| 4.9 | 0.181 ± 0.001 | 0.125 ± 0.003 | 36.3 ± 0.9 | 0.220 ± 0.003 | 1.840 ± 0.160 | 3.0 ± 0.2 | 0.189 ± 0.001 | 0.211 ± 0.002 | 22.5 ± 0.2 |
| 7.7 | 0.220 ± 0.003 | 0.113 ± 0.003 | 48.5 ± 0.8 | 0.310 ± 0.008 | 4.090 ± 0.070 | 1.9 ± 0.0 | 0.234 ± 0.0003 | 0.213 ± 0.005 | 27.5 ± 0.7 |
| 9.2 | 0.172 ± 0.001 | 0.125 ± 0.001 | 34.7 ± 0.1 | 0.239 ± 0.002 | 2.735 ± 0.159 | 2.2 ± 0.1 | 0.182 ± 0.0005 | 0.257 ± 0.003 | 17.7 ± 0.1 |
| 10.0 | 0.227 ± 0.002 | 0.105 ± 0.002 | 54.2 ± 1.1 | 0.400 ± 0.033 | 8.692 ± 1.855 | 1.7 ± 0.1 | 0.248 ± 0.0012 | 0.245 ± 0.011 | 25.3 ± 1.0 |
| 14.5 | 0.291 ± 0.004 | 0.126 ± 0.003 | 57.9 ± 1.2 | 0.513 ± 0.025 | 10.483 ± 1.797 | 1.2 ± 0.2 | 0.322 ± 0.008 | 0.301 ± 0.011 | 26.7 ± 0.6 |
| 18.5 | 0.186 ± 0.002 | 0.094 ± 0.003 | 49.7 ± 1.2 | 0.274 ± 0.022 | 3.668 ± 1.014 | 1.9 ± 0.3 | 0.192 ± 0.0008 | 0.163 ± 0.009 | 29.6 ± 1.6 |